

Physics impact of ILC Higgs coupling measurements: the effect of theory uncertainties

Andrew Droll¹ and Heather E. Logan^{1,*}

¹*Ottawa-Carleton Institute for Physics,
Carleton University, Ottawa K1S 5B6 Canada*

Abstract

We study the effect of theoretical and parametric uncertainties on the ability of future Higgs coupling measurements at the International Linear Collider (ILC) to reveal deviations from the Standard Model (SM). To quantify the impact of these uncertainties we plot $\Delta\chi^2 = 25$ contours for the deviations between the SM Higgs couplings and the light Higgs couplings in the m_h^{\max} benchmark scenario of the Minimal Supersymmetric Standard Model (MSSM). We consider the theoretical uncertainties in the SM Higgs decay partial widths and production cross section and the parametric uncertainties in the bottom and charm masses and the strong coupling α_s . We find that the impact of the theoretical and parametric uncertainties is moderate in the first phase of ILC data-taking (500 fb⁻¹ at 350 GeV centre-of-mass energy), reducing the “reach” in the CP-odd MSSM Higgs mass M_A by about 10% to ~ 500 GeV, while in the second phase (1000 fb⁻¹ at 1000 GeV) these uncertainties are larger than the experimental uncertainties and reduce the reach in M_A by about a factor of two, from ~ 1200 down to ~ 600 GeV. The bulk of the effect comes from the parametric uncertainties in m_b and α_s , followed by the theoretical uncertainty in Γ_b .

*Electronic address: logan@physics.carleton.ca

I. INTRODUCTION

An important component of the physics case for the International Linear Collider (ILC) is its ability to perform high-precision measurements in the Higgs sector [1, 2, 3]. In addition to measuring the Higgs mass, its spin and CP quantum numbers, and its self-coupling which characterizes the shape of the Higgs potential, the ILC will measure the Higgs couplings to a variety of Standard Model (SM) particles. In the SM, the masses of these particles arise solely through their couplings to the Higgs, so that these couplings are predicted in terms of the corresponding SM particle masses. The SM Higgs production cross sections and decay branching ratios are then fixed once the Higgs mass has been measured.

In extended models, however, the masses of the SM particles can receive contributions from more than one source, e.g., from couplings to each of two Higgs doublets. Further, the SM-like Higgs boson in extended models is typically an admixture of states from different scalar multiplets, leading to modifications of its couplings to SM particles by additional mixing angles. The high-precision ILC measurements of Higgs couplings thus provide a powerful tool for probing the structure of the Higgs sector and distinguishing the minimal SM from extended models.

Previous studies [4, 5, 6, 7, 8] have quantified the “reach” of the ILC measurements within the context of the Minimal Supersymmetric Standard Model (MSSM). In this paper we study the impact on this reach due to the theoretical and parametric uncertainties that enter the SM predictions for the Higgs cross section and decay branching ratios. A first attempt at including the parametric uncertainties from the strong coupling and the bottom and charm quark masses was made in Ref. [5] by varying these parameters within their uncertainties and treating the resulting variation in the SM Higgs branching ratio predictions as an additional uncertainty to be added in quadrature with the uncertainty on the experimental measurement. An additional step was taken in Ref. [9] where the theoretical uncertainties in the SM $\gamma\gamma \rightarrow H \rightarrow b\bar{b}$ rate were estimated based on the size of the computed radiative corrections. We refine and extend the analysis of the parametric uncertainties by taking into account their correlated effects on Higgs observables. We also include the full set of current theoretical uncertainties in the SM Higgs decay partial widths and production cross section, again taking into account their correlated effects on the ILC Higgs observables.

With the theoretical and parametric uncertainties in hand, we must choose a measure to

quantify their impact. We choose to work in the m_h^{\max} benchmark scenario of the MSSM as defined in Ref. [10]. We scan over points in the M_A - $\tan\beta$ plane and construct a chi-squared (χ^2) observable between the SM and MSSM predictions. We plot contours of $\Delta\chi^2 = 25$, corresponding to a 5σ discrepancy between the SM and the sample MSSM point. These contours allow us to show the impact of adding each of the theoretical and parametric uncertainties on top of the experimental uncertainties. Because the main purpose of this paper is to examine the impact of the theoretical uncertainties, we make no attempt to scan over more general sets of MSSM parameters or over non-supersymmetric models.

We begin in the next section with a brief overview of the MSSM Higgs couplings. framework of our analysis. In Sec. III we describe our χ^2 procedure for dealing with the uncorrelated and correlated sources of uncertainty. In Sec. IV we collect the expected experimental uncertainties in the Higgs measurements and describe our treatment of the theoretical and parametric uncertainties, which typically feed in to multiple measurements in a correlated way. We provide a table of the dependence of individual Higgs decay partial widths on the input parameters m_b , m_c and α_s so that our study can be updated in a straightforward way if the precision on these parameters improves. We present our numerical results in Sec. V. Section VI is reserved for discussion and conclusions. The current state of the art for the radiative corrections to SM Higgs decays, Higgs production in $e^+e^- \rightarrow \nu\bar{\nu}H$, and the bottom and charm quark mass extraction from low-energy experimental data is reviewed in Appendices A, B, and C, respectively.

II. THEORETICAL FRAMEWORK

The couplings of the lightest CP-even Higgs boson h^0 of the MSSM can be written at tree level in terms of the corresponding SM Higgs couplings as

$$\begin{aligned} \frac{g_{h^0\bar{t}t}}{g_{H_{\text{SM}}\bar{t}t}} &= \frac{g_{h^0\bar{c}c}}{g_{H_{\text{SM}}\bar{c}c}} = \sin(\beta - \alpha) + \cot\beta \cos(\beta - \alpha) \\ \frac{g_{h^0\bar{b}b}}{g_{H_{\text{SM}}\bar{b}b}} &= \frac{g_{h^0\tau\tau}}{g_{H_{\text{SM}}\tau\tau}} = \sin(\beta - \alpha) - \tan\beta \cos(\beta - \alpha) \\ \frac{g_{h^0WW}}{g_{H_{\text{SM}}WW}} &= \frac{g_{h^0ZZ}}{g_{H_{\text{SM}}ZZ}} = \sin(\beta - \alpha), \end{aligned} \tag{1}$$

where α is the mixing angle that diagonalizes the mass matrix for the CP-even states h^0 and H^0 , and $\tan \beta = v_2/v_1$ is the ratio of vacuum expectation values of the two MSSM Higgs doublets. At tree level we have

$$\cos(\beta - \alpha) \simeq \frac{1}{2} \sin 4\beta \frac{m_Z^2}{M_A^2}, \quad (2)$$

where M_A is the mass of the CP-odd neutral MSSM Higgs boson. Note that in the *decoupling limit* $M_A \gg m_Z$ [11], $\cos(\beta - \alpha)$ goes to zero and the h^0 couplings approach their SM values. Using Eqs. (1) and (2) to expand the Higgs partial widths in powers of m_Z^2/M_A^2 , we obtain [5]

$$\begin{aligned} \frac{\delta\Gamma_W}{\Gamma_W} = \frac{\delta\Gamma_Z}{\Gamma_Z} &\simeq -\frac{1}{4} \sin^2 4\beta \frac{m_Z^4}{M_A^4} \simeq -4 \cot^2 \beta \frac{m_Z^4}{M_A^4} \\ \frac{\delta\Gamma_b}{\Gamma_b} &\simeq \frac{\delta\Gamma_\tau}{\Gamma_\tau} \simeq -\tan \beta \sin 4\beta \frac{m_Z^2}{M_A^2} \simeq +4 \frac{m_Z^2}{M_A^2} \\ \frac{\delta\Gamma_c}{\Gamma_c} &\simeq \cot \beta \sin 4\beta \frac{m_Z^2}{M_A^2} \simeq -4 \cot^2 \beta \frac{m_Z^2}{M_A^2}, \end{aligned} \quad (3)$$

where the last equality in each line uses the large $\tan \beta$ approximation $\sin 4\beta \simeq -4 \cot \beta$. In particular, for large $\tan \beta$, Γ_b and Γ_τ exhibit the largest deviations from their SM values, while Γ_W approaches its SM value very quickly with increasing M_A .

Beyond tree level, the Higgs couplings receive radiative corrections, which mainly impact the CP-even Higgs mass matrix [12]. These can be taken into account by defining an effective mixing angle α_{eff} for use in place of α in the above formulas. Significant radiative corrections can also appear in the $h^0 \bar{b}b$ vertex due to squark-gluino loops, with their dominant piece parameterized as Δ_b [12]. Including this vertex correction, the $h^0 \bar{b}b$ coupling can be written as [5]

$$\frac{g_{h^0 \bar{b}b}}{g_{H_{\text{SM}} \bar{b}b}} = [\sin(\beta - \alpha) - \tan \beta \cos(\beta - \alpha)] \frac{1 - \Delta_b \cot \alpha \cot \beta}{1 + \Delta_b}. \quad (4)$$

In the limit of large M_A , $\cot \alpha \cot \beta \rightarrow -1$ and the Δ_b corrections also decouple.

In this paper we make our χ^2 comparisons using the implementations of the SM and MSSM Higgs couplings in the public Fortran code **HDECAY** [13]. **HDECAY** computes the h^0 couplings using the α_{eff} approximation, incorporating also the potentially significant Δ_b corrections to the $h^0 \bar{b}b$ coupling. For the loop-induced couplings of h^0 to photon or gluon

pairs, **HDECAY** includes the shift in the contribution from SM particles in the loop¹ due to the modified couplings in Eq. (1), as well as the new contributions to the amplitude from supersymmetric particles running in the loop and from the charged Higgs boson for $h^0 \rightarrow \gamma\gamma$. For comparisons involving MSSM Higgs production cross sections in WW fusion and ZH associated production, we scale the corresponding SM production cross section by $g_{h^0 VV}^2/g_{H_{\text{SM}} VV}^2$ ($V = W$ or Z) using the α_{eff} approximation of **HDECAY**. We neglect the additional non-universal SUSY electroweak radiative corrections (e.g., box diagrams) beyond this approximation. While a full MSSM analysis should include complete non-universal SUSY corrections to Higgs partial widths and production cross sections, the approximations used in **HDECAY** are sufficient for our purposes in this paper.

III. CHI-SQUARED ANALYSIS

To quantify the impact of the experimental and theoretical uncertainties on the ability of ILC measurements to reveal deviations from the SM, we construct a χ^2 according to

$$\chi^2 = \sum_{i=1}^n \sum_{j=1}^n (Q_i^{M_1} - Q_i^{M_2}) [\sigma^2]_{ij}^{-1} (Q_j^{M_1} - Q_j^{M_2}), \quad (5)$$

where Q_i are the observables being compared between models M_1 and M_2 , and $[\sigma^2]_{ij}^{-1}$ is the inverse of the covariance matrix for the quantities Q_i , defined according to

$$\sigma_{ij}^2 = \delta_{ij} u_i u_j + \sum_{k=1}^m c_i^k c_j^k. \quad (6)$$

Here u_i is the uncorrelated uncertainty in the observable Q_i , c_i^k represents the k th source of correlated uncertainty in Q_i , and δ_{ij} is the Kronecker delta. In the absence of correlated uncertainties, σ_{ij}^2 is a diagonal matrix with the (positive definite) squares of the uncorrelated uncertainties u_i down the diagonal. Correlated uncertainties introduce off-diagonal terms, which can be positive or negative depending on the sense of the correlation between observables Q_i and Q_j .

¹ We added the charm quark loop to the SM Γ_{gg} calculation in **HDECAY**, to be consistent with its inclusion in the MSSM calculation.

In our analysis the observables Q_i consist of Higgs branching fractions and Higgs production cross sections times branching fractions (i.e., rates in a particular channel). We take the expected experimental uncertainties on these quantities at the ILC from the literature. Because the existing experimental studies have not quantified the correlations between the measured observables, we treat the experimental uncertainties as uncorrelated. The theoretical and parametric uncertainties affect multiple observables, and we therefore treat them as correlated uncertainties.

IV. INPUTS

A. Experimental inputs

We consider Higgs measurements from two stages of ILC running:

- **Phase 1:** 500 fb⁻¹ of integrated luminosity at 350 GeV centre-of-mass energy, with no beam polarization. Expected uncertainties in the SM Higgs branching ratios for Higgs masses $m_H = 120$ and 140 GeV are taken from Ref. [14] and summarized in Table I.
- **Phase 2:** 1000 fb⁻¹ of integrated luminosity at 1000 GeV centre-of-mass energy, with beam polarizations of -80% for electrons and $+50\%$ for positrons. Expected uncertainties in the SM Higgs production cross section times branching ratios for $m_H = 115, 120$ and 140 GeV are taken from Ref. [15] and summarized in Table II. For the Phase 2 analysis, we include the existing Phase 1 measurements in the χ^2 in addition to the new measurements at 1000 GeV.

The centre-of-mass energy of 350 GeV was chosen for the study in Ref. [14] because it is near the peak of the $e^+e^- \rightarrow ZH$ cross section for the Higgs masses considered. It is also near the top quark pair production threshold, so that the Higgs data could be collected simultaneously with a top threshold scan. Running with polarized beams would improve the results by boosting the cross section and/or suppressing backgrounds. The actual ILC run plan will of course depend on what is discovered at the CERN Large Hadron Collider (LHC), and may include multiple threshold scans or running at the maximal first-phase design energy of 500 GeV.

SM Higgs branching ratio uncertainties from 500 fb ⁻¹ at 350 GeV		
	$m_H = 120$ GeV	140 GeV
BR($b\bar{b}$)	2.4%	2.6%
BR($c\bar{c}$)	8.3%	19.0%
BR($\tau\tau$)	5.0%	8.0%
BR(WW)	5.1%	2.5%
BR(gg)	5.5%	14.0%

TABLE I: Expected fractional experimental uncertainties in the SM Higgs branching ratios for $m_H = 120$ and 140 GeV, from Ref. [14] (500 fb⁻¹ at 350 GeV centre-of-mass energy with no beam polarization).

SM Higgs cross section times BR statistical uncertainties from 1000 fb ⁻¹ at 1000 GeV			
	$m_H = 115$ GeV		120 GeV
			140 GeV
$\sigma \times \text{BR}(b\bar{b})$	0.3%	0.4%	0.5%
$\sigma \times \text{BR}(WW)$	2.1%	1.3%	0.5%
$\sigma \times \text{BR}(gg)$	1.4%	1.5%	2.5%
$\sigma \times \text{BR}(\gamma\gamma)$	5.3%	5.1%	5.9%

TABLE II: Expected fractional experimental uncertainties in the SM Higgs production cross section times decay branching ratios for $m_H = 115$, 120 and 140 GeV, from Ref. [15] (1000 fb⁻¹ at 1000 GeV centre-of-mass energy). Uncertainties are statistical only. Beam polarizations of -80% for electrons and $+50\%$ for positrons are assumed.

The study in Ref. [15] at 1000 GeV centre-of-mass energy found the expected statistical uncertainties on Higgs rates in various channels. The analysis selected events with $e^+e^- \rightarrow \nu\bar{\nu}H$, thus including Higgs production via WW fusion and via $e^+e^- \rightarrow ZH$ with $Z \rightarrow \nu\bar{\nu}$. The Higgs decay products were then selected with the requirement that the visible energy in the event add up to the Higgs mass. The study in Ref. [15] evaluated the statistical uncertainties only. In our χ^2 analysis we add an overall luminosity uncertainty of 0.1% [1] for the Higgs rate measurements at 1000 GeV, completely correlated among the four channels. In this high-energy phase of ILC running, Higgs production is dominated by WW fusion, the cross section for which grows with centre-of-mass energy for a fixed m_H . It is thus advantageous to run at the highest possible collider energy to maximize the statistics. Beam polarization was chosen to maximize the WW fusion cross section.

In our analysis we scan over the $M_A\text{-tan}\beta$ plane in the m_h^{max} scenario of the MSSM. At each parameter point we take the Higgs observables for h^0 and those for a SM Higgs boson of the same mass as the input for our χ^2 . For Higgs masses between 120 and 140 GeV, we obtain

Higgs partial width	Theory uncertainty	
	in literature	in HDECAY
$\Gamma_{b\bar{b}}, \Gamma_{c\bar{c}}$	1%	1%
$\Gamma_{\tau\tau}, \Gamma_{\mu\mu}$	0.01%	0.01%
Γ_{WW}, Γ_{ZZ}	0.5%	5%
Γ_{gg}	3%	16%
$\Gamma_{\gamma\gamma}$	0.1%	4%
$\Gamma_{Z\gamma}$	4%	4%
Higgs production cross section		
$\sigma_{e^+e^- \rightarrow \nu\bar{\nu}H}$	0.5%	—

TABLE III: Estimated fractional theoretical uncertainties in the SM Higgs partial widths and production cross section due to uncalculated higher order corrections. See Appendices A and B for details.

the expected experimental uncertainty on the Higgs observables using linear interpolation between the values given in Tables I and II. In the m_h^{\max} scenario the h^0 mass never exceeds 130 GeV. For h^0 masses below 120 GeV, which occur in this scenario only at low $\tan\beta$ values < 4 , we use the experimental uncertainties for $m_H = 120$ GeV from Table I and apply linear interpolation only to the values given in Table II between $m_H = 115$ and 120 GeV.

B. Theoretical and parametric uncertainties

1. Higgs decay partial widths

The theoretical uncertainties in the SM Higgs decay partial widths due to uncalculated higher order radiative corrections are summarized in Table III. We estimated these numbers based on the size of the known higher order corrections for Higgs masses in our range of interest; for details see Appendix A. In all cases we use the best theory uncertainty available in the literature for our χ^2 calculation; in some cases the theory uncertainty in the HDECAY calculation is larger because not all available radiative corrections have been implemented into the HDECAY code [16].

Working entirely in terms of fractional uncertainties, the correlated uncertainty c_i^k in branching ratio i due to the theoretical uncertainty in the SM prediction for partial width k is given by the formula

$$c_i^k = \frac{\Gamma_k}{\text{BR}_i} \frac{\partial \text{BR}_i}{\partial \Gamma_k} \sigma_{\Gamma_k}, \quad (7)$$

Parameter	Value	Percent uncertainty	Source
$\alpha_s(m_Z)$	0.1185 ± 0.0020	1.7%	[20]
$\overline{m}_b(M_b)$	$4.20 \pm 0.04 \text{ GeV}$	0.95%	[21]
$\overline{m}_c(M_c)$	$1.224 \pm 0.057 \text{ GeV}$	4.7%	[22]

TABLE IV: Central values and uncertainties of α_s and the $\overline{\text{MS}}$ bottom and charm quark masses $\overline{m}_b(M_b)$ and $\overline{m}_c(M_c)$ used in the analysis.

where σ_{Γ_k} is the (fractional) theoretical uncertainty on partial width Γ_k . The normalized derivatives are given analytically by

$$\frac{\Gamma_k}{\text{BR}_i} \frac{\partial \text{BR}_i}{\partial \Gamma_k} = \begin{cases} -\text{BR}_k & \text{for } i \neq k \\ (1 - \text{BR}_k) & \text{for } i = k. \end{cases} \quad (8)$$

2. Cross section for $e^+e^- \rightarrow \nu\bar{\nu}H$

At 1000 GeV centre-of-mass energy the production cross section for $e^+e^- \rightarrow \nu\bar{\nu}H$ is dominated by WW fusion, with a subleading contribution from $e^+e^- \rightarrow ZH$ with $Z \rightarrow \nu\bar{\nu}$. The SM cross section is currently known including the one-loop electroweak radiative corrections [17, 18, 19]. We take the remaining theoretical uncertainty in the cross section to be 0.5%; see Appendix B for details. This cross section uncertainty is included in the χ^2 calculation in the same way as the luminosity uncertainty discussed earlier, completely correlated among the four rate measurements.

3. α_s , $\overline{m}_b(M_b)$, and $\overline{m}_c(M_c)$

The most important sources of parametric uncertainties in the SM Higgs coupling calculations are the strong coupling α_s and the bottom and charm quark masses. The input values used in our analysis are summarized in Table IV. For α_s we use the current world average from the Particle Data Group [20]. For the bottom and charm quark masses we use the values from fits to the kinematic moments in inclusive semileptonic B meson decays; details are given in Appendix C. We make the approximation that the $\overline{\text{MS}}$ quark mass $\overline{m}_q(M_q)$ evaluated at the corresponding quark pole mass M_q (used by `HDECAY`) is the same as the mass $\overline{m}_q(\overline{m}_q)$ evaluated at its own running mass (extracted from the B decay fits).

We implement the parametric uncertainties in the χ^2 calculation as follows. Again, all

uncertainties are fractional. The correlated uncertainty $c_i^{x_j}$ in branching ratio i due to the parametric uncertainty in $x_j \in \{\alpha_s(m_Z), \overline{m}_b(M_b), \overline{m}_c(M_c)\}$ is given by

$$c_i^{x_j} = \frac{x_j}{\text{BR}_i} \frac{\partial \text{BR}_i}{\partial x_j} \sigma_{x_j} = \sum_{k=1}^n \left[\frac{\Gamma_k}{\text{BR}_i} \frac{\partial \text{BR}_i}{\partial \Gamma_k} \right] \left[\frac{x_j}{\Gamma_k} \frac{\partial \Gamma_k}{\partial x_j} \right] \sigma_{x_j}, \quad (9)$$

where σ_{x_j} is the (fractional) uncertainty on the parameter x_j . The second equality was obtained using the chain rule; the first term inside the sum was given explicitly in Eq. (8).

The calculation thus consists of evaluating the derivatives $\partial \Gamma_k / \partial x_j$ while holding constant all the parameters other than x_j . In principle, this can be done by varying each of the inputs x_j in **HDECAY** and reading off the resulting variation in Γ_k . This is complicated by the fact that **HDECAY** takes as inputs not the running masses $\overline{m}_b(M_b)$ and $\overline{m}_c(M_c)$, but the pole masses M_b and M_c themselves. Varying M_b while holding M_c constant is not the same as varying $\overline{m}_b(M_b)$ while holding $\overline{m}_c(M_c)$ constant; likewise, varying $\alpha_s(m_Z)$ while holding M_b and M_c constant results in a variation of $\overline{m}_b(M_b)$ and $\overline{m}_c(M_c)$.

To deal with this, we use the chain rule and next-to-leading-order (NLO) approximations. We start by writing the quark pole masses as functions of our desired input parameters: $M_b = M_b(\overline{m}_b, \alpha_s)$ and $M_c = M_c(\overline{m}_b, \overline{m}_c, \alpha_s)$, where the running quark masses are understood to be evaluated at their corresponding pole mass scales and $\alpha_s \equiv \alpha_s(m_Z)$. Any Higgs partial width Γ can then be expressed as $\Gamma = \Gamma(M_b(\overline{m}_b, \alpha_s), M_c(\overline{m}_b, \overline{m}_c, \alpha_s), \alpha_s)$. The chain rule then gives

$$\begin{aligned} \left. \frac{\partial \Gamma}{\partial \overline{m}_b} \right|_{\overline{m}_c, \alpha_s} &= \left. \frac{\partial \Gamma}{\partial M_b} \right|_{M_c, \alpha_s} \left. \frac{\partial M_b}{\partial \overline{m}_b} \right|_{\alpha_s} + \left. \frac{\partial \Gamma}{\partial M_c} \right|_{M_b, \alpha_s} \left. \frac{\partial M_c}{\partial \overline{m}_b} \right|_{\overline{m}_c, \alpha_s} \\ \left. \frac{\partial \Gamma}{\partial \overline{m}_c} \right|_{\overline{m}_b, \alpha_s} &= \left. \frac{\partial \Gamma}{\partial M_c} \right|_{M_b, \alpha_s} \left. \frac{\partial M_c}{\partial \overline{m}_c} \right|_{\overline{m}_b, \alpha_s} \\ \left. \frac{\partial \Gamma}{\partial \alpha_s} \right|_{\overline{m}_b, \overline{m}_c} &= \left. \frac{\partial \Gamma}{\partial \alpha_s} \right|_{M_b, M_c} + \left. \frac{\partial \Gamma}{\partial M_b} \right|_{M_c, \alpha_s} \left. \frac{\partial M_b}{\partial \alpha_s} \right|_{\overline{m}_b} + \left. \frac{\partial \Gamma}{\partial M_c} \right|_{M_b, \alpha_s} \left. \frac{\partial M_c}{\partial \alpha_s} \right|_{\overline{m}_b, \overline{m}_c}. \end{aligned} \quad (10)$$

HDECAY can be used in a straightforward way to numerically evaluate $[\partial \Gamma / \partial M_b]_{M_c, \alpha_s}$, $[\partial \Gamma / \partial M_c]_{M_b, \alpha_s}$, and $[\partial \Gamma / \partial \alpha_s]_{M_b, M_c}$. We did this by varying each of the input parameters M_b , M_c , and α_s about its central value over a range of approximately twice its uncertainty as given in Table IV. We also checked explicitly that the dependence of each of the partial widths was linear under these (small) variations.

We evaluate the remaining derivatives analytically as follows. The relation between the pole mass M_q and running mass $\overline{m}_q \equiv \overline{m}_q(M_q)$ at NLO is

$$M_q = \overline{m}_q \left[1 + \frac{4}{3\pi} \alpha_s(M_q) \right]. \quad (11)$$

Differentiating this with respect to \overline{m}_q yields

$$\frac{\partial M_q}{\partial \overline{m}_q} = 1 + \frac{4}{3\pi} \alpha_s(M_q) + \overline{m}_q \frac{4}{3\pi} \frac{\partial \alpha_s(M_q)}{\partial \overline{m}_q}. \quad (12)$$

The derivative of α_s can be found from the NLO formula

$$\alpha_s(M_q) = \frac{\alpha_s(\mu)}{1 + (b/2\pi) \alpha_s(\mu) \log(M_q/\mu)}, \quad (13)$$

where $b = 11 - 2N_f/3$ and N_f is the number of active quark flavours in the running of α_s between the scales μ and M_q . In particular, $\partial \alpha_s(M_q)/\partial \overline{m}_q = \mathcal{O}(\alpha_s^2)$; working to NLO we will neglect this term. The derivative of interest then becomes

$$\frac{\partial M_q}{\partial \overline{m}_q} \simeq 1 + \frac{4}{3} \alpha_s(M_q) = \frac{M_q}{\overline{m}_q}, \quad (14)$$

i.e., the normalized derivative $(\overline{m}_q/M_q)(\partial M_q/\partial \overline{m}_q) = 1$ at NLO. A similar calculation yields $\partial M_c/\partial \overline{m}_b = 0$ at NLO.

The derivatives of the quark pole masses with respect to α_s are evaluated as follows. From Eq. (11) we have, to NLO,

$$\frac{\partial M_q}{\partial \alpha_s(m_Z)} = \overline{m}_q \frac{4}{3\pi} \frac{\partial \alpha_s(M_q)}{\partial \alpha_s(m_Z)}. \quad (15)$$

Equation (13) can be used to evaluate the α_s derivative at NLO,²

$$\frac{\partial \alpha_s(M_q)}{\partial \alpha_s(m_Z)} = \left[\frac{\alpha_s(M_q)}{\alpha_s(m_Z)} \right]^2. \quad (16)$$

² This formula automatically takes into account the change in the number of quark flavours in the running at the b threshold.

Normalized derivatives of Higgs partial widths									
	$\alpha_s(m_Z)$			$\overline{m}_b(M_b)$			$\overline{m}_c(M_c)$		
m_H	120 GeV	140 GeV	160 GeV	120 GeV	140 GeV	160 GeV	120 GeV	140 GeV	160 GeV
$\Gamma_{b\bar{b}}$	-1.177	-1.217	-1.249	2.565	2.567	2.568	0.000	0.000	0.000
$\Gamma_{c\bar{c}}$	-4.361	-4.400	-4.432	-0.083	-0.084	-0.084	3.191	3.192	3.192
Γ_{gg}	2.277	2.221	2.175	-0.114	-0.112	-0.104	-0.039	-0.032	-0.027
$\Gamma_{\gamma\gamma}$	0.002	0.002	0.001	0.010	0.008	0.005	0.012	0.009	0.005

TABLE V: Normalized derivatives, $(x/\Gamma)(\partial\Gamma/\partial x)$, of SM Higgs partial widths with respect to the parameters $\alpha_s(m_Z)$, $\overline{m}_b(M_b)$, and $\overline{m}_c(M_c)$ for $m_H = 120, 140$, and 160 GeV. See text for details. The central values of the three input parameters were taken from Table IV.

Combining Eqs. (15) and (16) we find for the normalized derivative,

$$\frac{\alpha_s(m_Z)}{M_q} \frac{\partial M_q}{\partial \alpha_s(m_Z)} = \frac{\overline{m}_q}{M_q} \frac{4}{3\pi} \alpha_s(M_q) \frac{\alpha_s(M_q)}{\alpha_s(m_Z)} \simeq \frac{4}{3\pi} \alpha_s(M_q), \quad (17)$$

where in the last step we keep only terms up to NLO.

The dependences of the SM Higgs partial widths Γ_i on variations in the inputs $x_j \in \{\alpha_s, \overline{m}_b(M_b), \overline{m}_c(M_c)\}$ are summarized in Table V in the form of normalized derivatives, $(x_j/\Gamma_i)(\partial\Gamma_i/\partial x_j)$, evaluated at the central values of the inputs x_j . For example, for $m_H = 120$ GeV, a 1% increase in $\overline{m}_b(M_b)$ leads to a 2.6% increase in $\Gamma_{b\bar{b}}$, while a 1% increase in $\alpha_s(m_Z)$ leads to a 1.2% decrease in $\Gamma_{b\bar{b}}$. The dependence of the normalized derivatives on the Higgs mass is not very strong. We again use linear interpolation to find the appropriate normalized derivatives for Higgs mass values between those given in Table V. Finally, we note that the Higgs partial widths to WW , ZZ , and lepton pairs, and the production cross section for $e^+e^- \rightarrow \nu\bar{\nu}H$, do not depend on α_s , $\overline{m}_b(M_b)$, or $\overline{m}_c(M_c)$.

The general pattern of the normalized derivatives in Table V can be understood as follows. The $H \rightarrow q\bar{q}$ partial widths are proportional to $\overline{m}_q^2(m_H)$ [see Eq. (A1)]. Neglecting QCD running of the quark mass, the normalized derivative of $\Gamma_{q\bar{q}}$ with respect to \overline{m}_q should thus be equal to 2. The values in Table V are actually somewhat larger than 2 because of the effect of QCD running, which causes $\overline{m}_q(\mu)$ to decrease as the scale μ increases. Raising $\overline{m}_q(M_q)$ by a small amount reduces the range of scales (from M_q to m_H) over which the QCD running is applied, so that $\overline{m}_q(m_H)$ is even larger than it would be just from the increase in $\overline{m}_q(M_q)$ without the effect of the running. This effect is more pronounced in $\Gamma_{c\bar{c}}$ than in $\Gamma_{b\bar{b}}$ because α_s is larger at the charm quark mass scale than at the bottom mass scale, resulting

in faster running for \overline{m}_c near the scale M_c . Similarly, increasing $\alpha_s(m_Z)$ strengthens the QCD running of \overline{m}_q , resulting in a reduction of $\Gamma_{q\bar{q}}$. Changing α_s also affects the QCD corrections to $\Gamma_{q\bar{q}}$; however, the dominant effect is absorbed already into the running quark mass.

The slight dependence of $\Gamma_{c\bar{c}}$ on $\overline{m}_b(M_b)$ is due to the effect of the b threshold on the running of \overline{m}_c . Adding the b quark to the renormalization group equations slows down the running of \overline{m}_c , so that increasing the b mass slightly reduces the high-scale value of \overline{m}_c and thus reduces $\Gamma_{c\bar{c}}$. Note that by working to NLO in evaluating the derivatives above, we have neglected contributions to the \overline{m}_b dependence of $\Gamma_{c\bar{c}}$ of the same order as those that give the dependence shown in Table V; a higher order treatment would thus give different results. However, the numerical effect of these terms is negligible, so we do not attempt a more precise evaluation here.

Γ_{gg} is proportional to α_s^2 at leading order. NLO QCD corrections increase Γ_{gg} rather significantly, leading to a normalized derivative somewhat larger than 2. Γ_{gg} is dominated in the SM by the top quark loop, so that the effect of varying $\overline{m}_b(M_b)$ and $\overline{m}_c(M_c)$ is small. The anticorrelation in this case is due to destructive interference between the real parts of the b and c quark loop amplitudes and the top quark loop amplitude.

Finally, the similar sensitivity of $\Gamma_{\gamma\gamma}$ to $\overline{m}_b(M_b)$ and $\overline{m}_c(M_c)$ can be understood by noting that the bottom and charm quark loops contribute mainly through their interference with the dominant top and W boson loops, and that their contributions go like $\overline{m}_b(m_H)Q_b^2$ and $\overline{m}_c(m_H)Q_c^2$, respectively, while $\overline{m}_b(\mu)/\overline{m}_c(\mu) \simeq 0.235 \pm 0.012$ [21] and $Q_c^2 = 4Q_b^2$ so that the two contributions are actually comparable.

V. RESULTS

Our main results are summarized in Fig. 1, where we plot $\Delta\chi^2 = 25$ contours for the deviations between the SM Higgs and the lighter CP-even Higgs in the m_h^{\max} scenario of the MSSM. To the left of these contours, the MSSM Higgs can be distinguished from the SM Higgs at more than the 5σ level. The dashed curves show the reach including experimental uncertainties only, while the solid curves show the effect of adding the theoretical and parametric uncertainties.

For the first phase of ILC running (the left pair of curves in Fig. 1; 500 fb^{-1} at 350

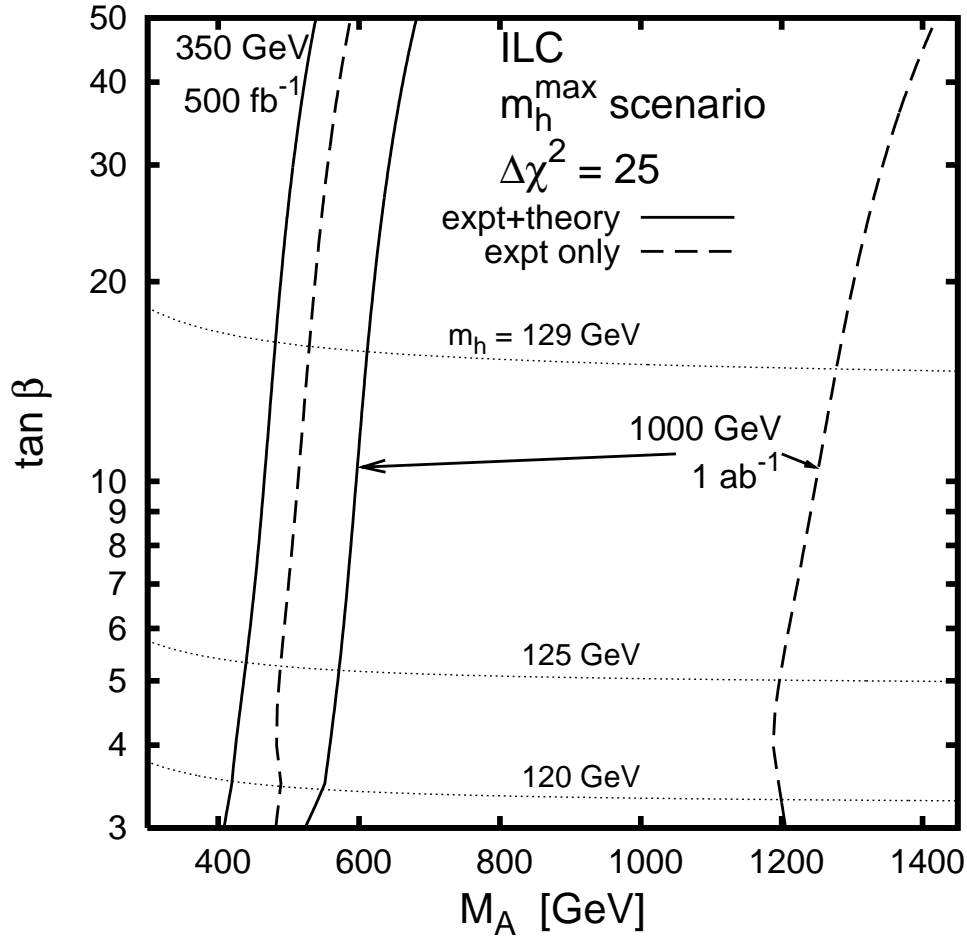


FIG. 1: Contours of $\Delta\chi^2 = 25$ from the experimental uncertainties only (dashed lines) and including all theoretical and parametric uncertainties (solid lines). The pair of contours on the left are for Phase 1 and the pair on the right are for Phase 2.

GeV, experimental uncertainties from Table I), the impact of the theoretical and parametric uncertainties is to reduce the reach in M_A by about 50 GeV, or roughly 10%. Details are shown in Figs. 2 and 3, where we plot separately the contribution of each source of parametric and theoretical uncertainty. The bulk of the effect is due to the parametric uncertainties in $\overline{m}_b(M_b)$ and $\alpha_s(m_Z)$, as shown in Fig. 2. Smaller contributions come from the theoretical uncertainty in Γ_b , and for low $\tan\beta \lesssim 6$ from the parametric uncertainty in $\overline{m}_c(M_c)$ and the theoretical uncertainty in Γ_g . The change with $\tan\beta$ is partly due to the decrease in m_h with decreasing $\tan\beta$, as shown by the horizontal dotted lines in Figs. 2 and 3.

The relative importance of the different branching fraction measurements in the first phase of ILC running is illustrated in Table VI. We list the fractional deviations of the MSSM

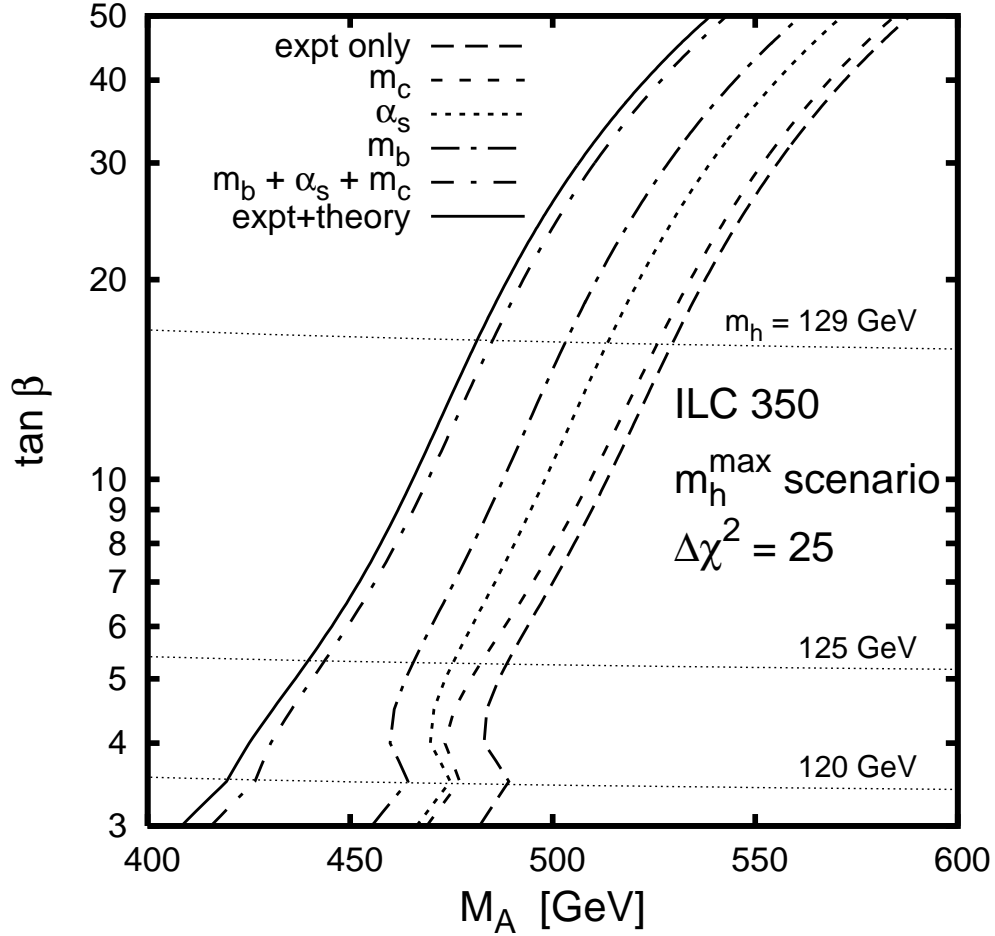


FIG. 2: Contributions of individual sources of parametric uncertainty to the $\Delta\chi^2 = 25$ contours in Phase 1.

Phase 1 sample point: $M_A = 537.6$ GeV, $\tan\beta = 20$						
Observable	Shift	Expt uncert	Pull	Thy+param uncert	Total uncert	Pull
BR($b\bar{b}$)	8.1%	2.5%	3.25	1.6%	3.0%	2.71
BR($c\bar{c}$)	-12.0%	13.2%	-0.90	16.1%	20.8%	-0.57
BR($\tau\tau$)	10.0%	6.4%	1.56	1.8%	6.6%	1.51
BR(WW)	-11.6%	3.9%	-2.96	1.8%	4.3%	-2.68
BR(gg)	-14.7%	9.4%	-1.56	5.8%	11.1%	-1.33

TABLE VI: Contributions to the $\Delta\chi^2$ at a Phase 1 sample point lying on the $\Delta\chi^2 = 25$ contour including only experimental uncertainties in Figs. 2 and 3. Shown are the fractional deviations in Higgs branching ratios in the m_h^{\max} scenario compared to the SM, the experimental uncertainties for the corresponding Higgs mass $m_h = 129.2$ GeV taken from a linear interpolation in Higgs mass between the values in Table I, the resulting “pulls,” i.e., the branching ratio deviations normalized by their experimental uncertainties, the combined theoretical and parametric uncertainties on the observables, the total uncertainty, and the resulting pull from the total uncertainty. Not shown are the off-diagonal elements of the correlation matrix due to the theoretical and parametric uncertainties.

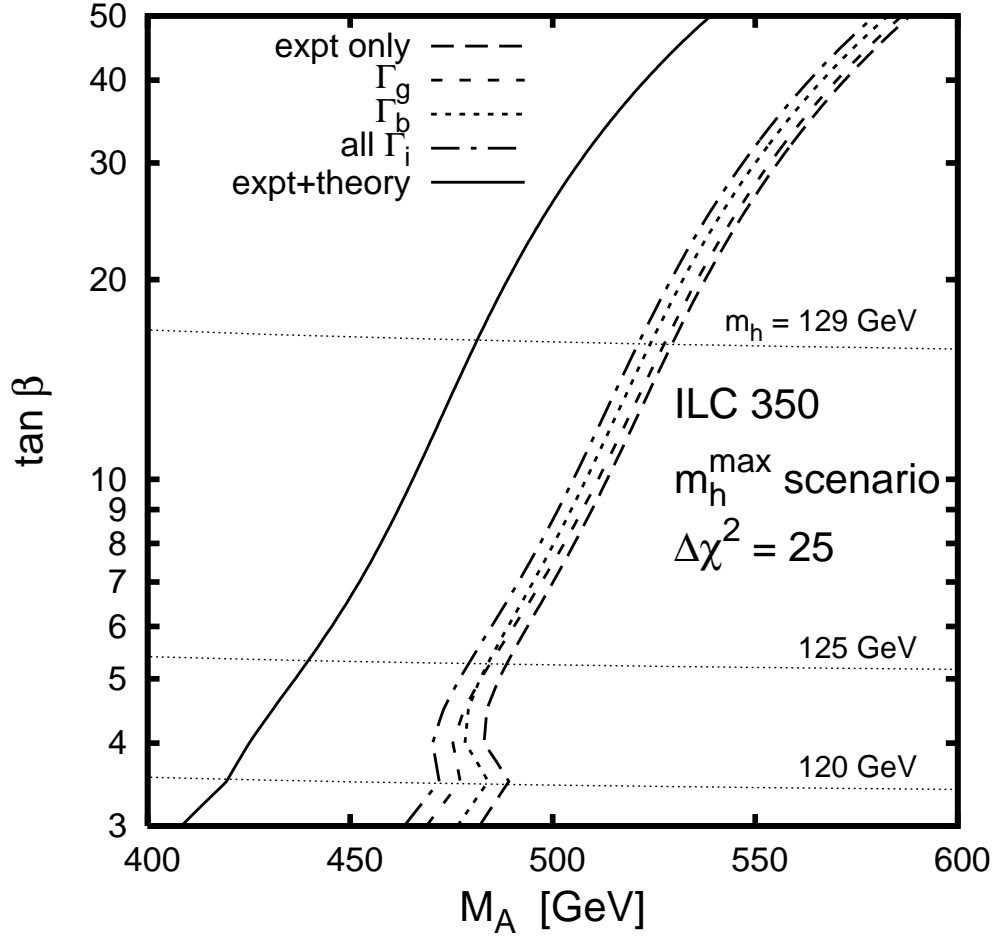


FIG. 3: Contributions of individual sources of theoretical uncertainty to the $\Delta\chi^2 = 25$ contours in Phase 1. The additional theory uncertainties not plotted separately have a negligible effect.

Higgs branching ratios from their SM values at the “Phase 1 sample point” $M_A = 537.6$ GeV and $\tan\beta = 20$, which lies on the $\Delta\chi^2 = 25$ contour from experimental uncertainties only and yields $m_h = 129.2$ GeV. The relevant branching fractions deviate by roughly 10% from their SM values at this sample point. The biggest contributions to the $\Delta\chi^2$ come from the best-measured branching fractions, $\text{BR}(b\bar{b})$ and $\text{BR}(WW)$. Including the theoretical and parametric uncertainties moderately degrades the precision in all the channels, reducing the $\Delta\chi^2$ from 25 down to 17.4 at the sample point. This $\Delta\chi^2$ is slightly worse than the value of 18.9 that would be obtained by summing the squares of the pulls in Table VI; this is due to the effect of the off-diagonal elements in the correlation matrix. The effects of the most important parametric uncertainties, in $\overline{m}_b(M_b)$ and $\alpha_s(m_Z)$, are anticorrelated between $\text{BR}(b\bar{b})$ and $\text{BR}(WW)$ and thus can mimic the anticorrelated shift in these observables that occurs in the MSSM.

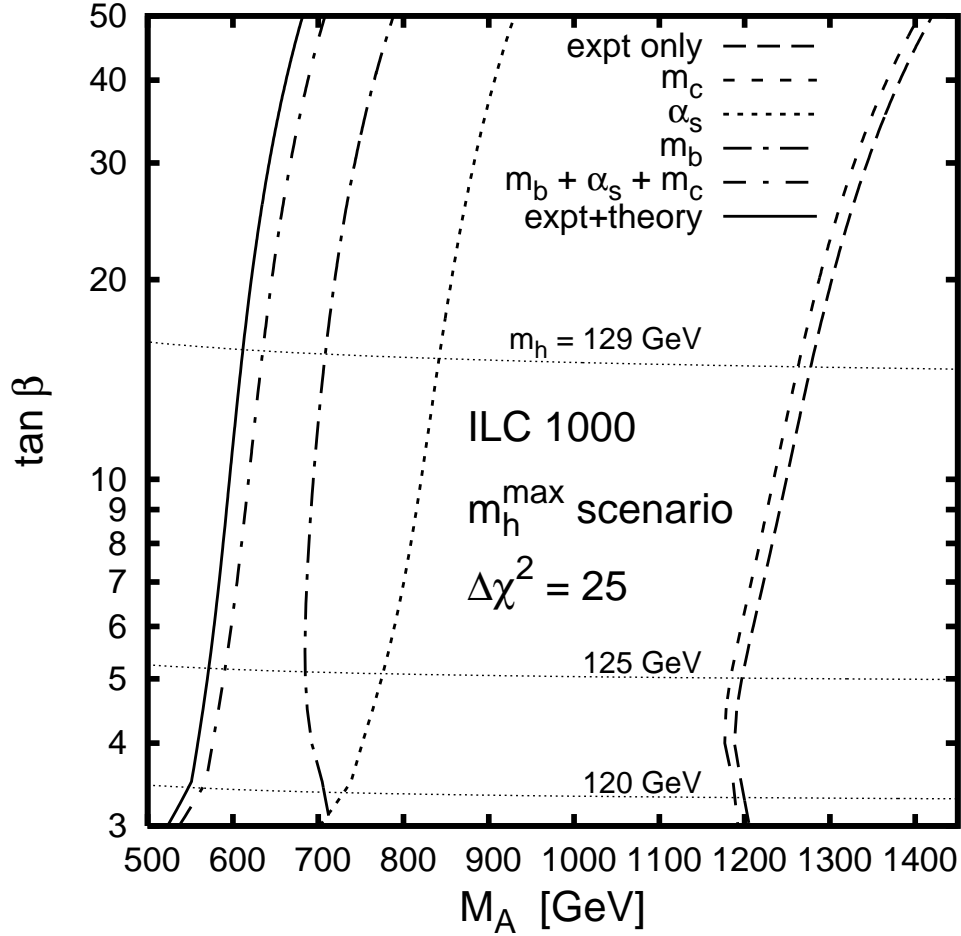


FIG. 4: Contributions of individual sources of parametric uncertainty to the $\Delta\chi^2 = 25$ contours in Phase 2.

For the second phase of ILC running (the right set of curves in Fig. 1; combining measurements from 1000 fb^{-1} at 1000 GeV and 500 fb^{-1} at 350 GeV, experimental uncertainties from Tables I and II), the experimental uncertainties are considerably smaller. The theoretical and parametric uncertainties thus have a much more significant impact: their effect is to reduce the reach in M_A by about a factor of two, from about 1200–1400 GeV down to about 525–700 GeV. Details are shown in Figs. 4 and 5. The dominant contributions by far are the parametric uncertainties in $\overline{m}_b(M_b)$ and $\alpha_s(m_Z)$ (Fig. 4), followed by the theoretical uncertainty in Γ_b and for low $\tan\beta \lesssim 4$ in Γ_g (Fig. 5).

The impact of the parametric and theoretical uncertainties on the individual channels used in the Phase 2 $\Delta\chi^2$ calculation is illustrated in Table VII. We list the fractional deviations of the MSSM Higgs observables from their SM values at the “Phase 2 sample point” $M_A = 1302.4 \text{ GeV}$ and $\tan\beta = 20$, which lies on the $\Delta\chi^2 = 25$ contour from experimental

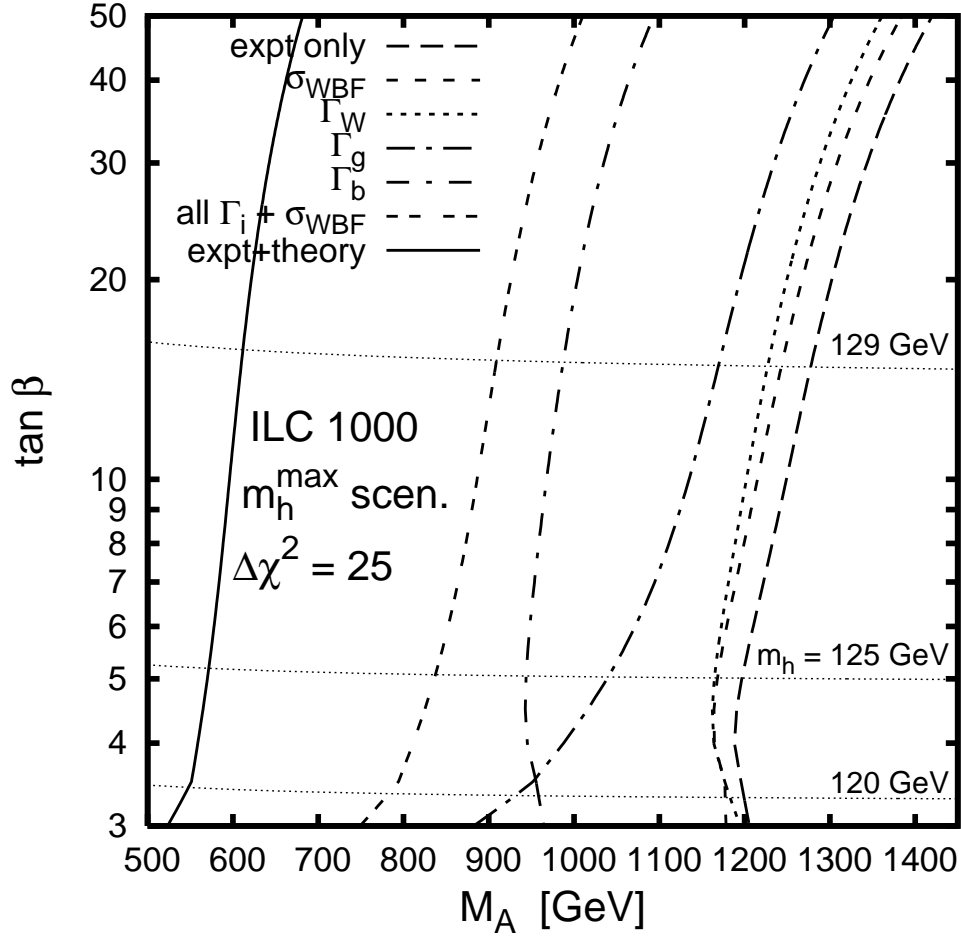


FIG. 5: Contributions of individual sources of theoretical uncertainty to the $\Delta\chi^2 = 25$ contours in Phase 2. The additional theory uncertainties not plotted separately have a negligible effect.

uncertainties only and yields $m_h = 129.3$ GeV. The relevant observables deviate by roughly 2% to 4% from their SM values at this sample point, except for $\sigma \times \text{BR}(\gamma\gamma)$ which is very close to its SM value. Ignoring the parametric and theoretical uncertainties, the biggest contribution to the $\Delta\chi^2$ comes from the best-measured observable, $\sigma \times \text{BR}(b\bar{b})$, followed by $\sigma \times \text{BR}(gg)$ and $\sigma \times \text{BR}(WW)$. The contribution of the branching fraction measurements from 350 GeV running to the $\Delta\chi^2$ is small.

Including the theoretical and parametric uncertainties severely degrades the precision of the three most important measurements, $\sigma \times \text{BR}(b\bar{b})$, $\sigma \times \text{BR}(WW)$, and $\sigma \times \text{BR}(gg)$, reducing the $\Delta\chi^2$ dramatically from 25 down to 1.7 at the sample point. This $\Delta\chi^2$ is somewhat worse than the value of 3.2 that would be obtained by summing the squares of the pulls in Table VII; this is again due to the effect of the off-diagonal elements in the correlation matrix, including the correlations between the Phase 1 branching ratio measurements and

Phase 2 sample point: $M_A = 1302.4$ GeV, $\tan\beta = 20$						
Observable	Shift	Expt uncert	Pull	Thy+param uncert	Total uncert	Pull
$\text{BR}(b\bar{b})$	1.7%	2.5%	0.67	1.7%	3.0%	0.55
$\text{BR}(c\bar{c})$	-2.5%	13.3%	-0.19	16.1%	20.8%	-0.12
$\text{BR}(\tau\tau)$	2.1%	6.4%	0.34	1.8%	6.6%	0.32
$\text{BR}(WW)$	-2.1%	3.9%	-0.53	1.8%	4.3%	-0.48
$\text{BR}(gg)$	-4.6%	9.4%	-0.48	5.8%	11.1%	-0.41
$\sigma \times \text{BR}(b\bar{b})$	1.7%	0.45%	3.72	1.7%	1.8%	0.93
$\sigma \times \text{BR}(WW)$	-2.1%	0.93%	-2.22	1.9%	2.1%	-0.98
$\sigma \times \text{BR}(gg)$	-4.6%	2.0%	-2.32	5.8%	6.2%	-0.74
$\sigma \times \text{BR}(\gamma\gamma)$	0.27%	5.5%	0.05	1.9%	5.8%	0.05

TABLE VII: Contributions to the $\Delta\chi^2$ at a Phase 2 sample point lying on the $\Delta\chi^2 = 25$ contour including only experimental uncertainties in Figs. 4 and 5. Shown are the fractional deviations in Higgs observables in the m_h^{max} scenario compared to the SM, the experimental uncertainties for the corresponding Higgs mass $m_h = 129.3$ GeV taken from a linear interpolation in Higgs mass between the values in Tables I and II, the resulting pulls, the combined theoretical and parametric uncertainties on the observables, the total uncertainty, and the resulting pull from the total uncertainty. Not shown are the off-diagonal elements of the correlation matrix due to the theoretical and parametric uncertainties.

the Phase 2 rate measurements.

VI. DISCUSSION AND CONCLUSIONS

We studied the impact of the theoretical and parametric uncertainties in the SM predictions for Higgs production and decay on the ability of the ILC to reveal deviations from the SM Higgs. To quantify the impact of the theoretical and parametric uncertainties, we compared the SM predictions for Higgs observables to those in the m_h^{max} benchmark scenario of the MSSM. We plotted $\Delta\chi^2 = 25$ contours for the deviations between the SM and MSSM Higgs observables both with and without the theory uncertainties, given the expected precisions on Higgs measurements at a future ILC. We found that the impact of the theoretical and parametric uncertainties is moderate in the first phase of ILC data-taking (500 fb⁻¹ at 350 GeV centre-of-mass energy), reducing the reach in the CP-odd MSSM Higgs mass M_A by about 10% to ~ 500 GeV, while in the second phase (1000 fb⁻¹ at 1000 GeV) these uncertainties are larger than the experimental uncertainties and reduce the reach in M_A by about a factor of two, from ~ 1200 down to ~ 600 GeV. The bulk of the effect comes from the parametric uncertainties in m_b and α_s , followed by the theoretical uncertainty in

Γ_b . The theoretical uncertainty in Γ_g is also important for lower Higgs masses below about 120–125 GeV.

The single most important source of theoretical or parametric uncertainty is the bottom quark mass. In our analysis we used the measurement of m_b from a global fit to inclusive semileptonic B meson decay spectra [21] (see Appendix C for details). This is currently the best measurement of m_b ; its uncertainty of 0.95% is dominated by the theoretical uncertainties in the fit. The large impact of this parametric uncertainty on Higgs observables is due to (i) the effective 2.6 power with which $\overline{m}_b(M_b)$ enters Γ_b , (ii) the importance of the $b\bar{b}$ final state in ILC Higgs measurements, and (iii) the fact that the deviations of the MSSM Higgs couplings from their SM values show up largely in the b and τ sectors. The impact of the uncertainty in m_b on the long-term ILC Higgs program highlights the need for further theoretical work on the m_b extraction from B meson observables.

The second most important source of theoretical or parametric uncertainty is $\alpha_s(m_Z)$. In our analysis we used the world-average PDG value [20] with an uncertainty of 0.0020 or 1.7%. This measurement is expected to be improved by at least a factor of two at the ILC through precision measurements of event shape observables, the cross section ratio $\sigma_{t\bar{t}}/\sigma_{\mu^+\mu^-}$ above the $t\bar{t}$ threshold, and $\Gamma_Z^{\text{had}}/\Gamma_Z^{\text{lept}}$ at the Z pole (via the GigaZ option) [1]. We illustrate the effect of improving the uncertainty on $\alpha_s(m_Z)$ to 0.0009 or 0.76% [1] in Fig. 6. By itself this improvement has a relatively small effect because the uncertainty is still dominated by m_b ; however, if the m_b extraction becomes significantly more precise, the improvement in α_s will be valuable.

The measurement of $\text{BR}(cc)$ did not contribute significantly to the $\Delta\chi^2$ because of its relatively poor experimental precision, particularly at the higher Higgs masses ~ 125 –130 GeV that appear over most of the m_h^{max} parameter space. Even if the ILC measurement were to be improved, however, the parametric uncertainties in $\overline{m}_c(M_c)$ and $\alpha_s(m_Z)$ lead to a large uncertainty in the SM prediction for $\text{BR}(cc)$ – 16% at our sample points – limiting the usefulness of this mode for model discrimination. The charm mass is by far the dominant uncertainty here, contributing 14.6%, while α_s contributes 6.4%. Note however that the theoretical improvements in B meson decays required to reduce the uncertainty in m_b will also reduce the uncertainty in m_c .

We also note here that the theoretical calculation of higher-order QCD corrections to $H \rightarrow gg$ includes processes in which one of the final-state gluons splits into a $c\bar{c}$ or $b\bar{b}$ pair.

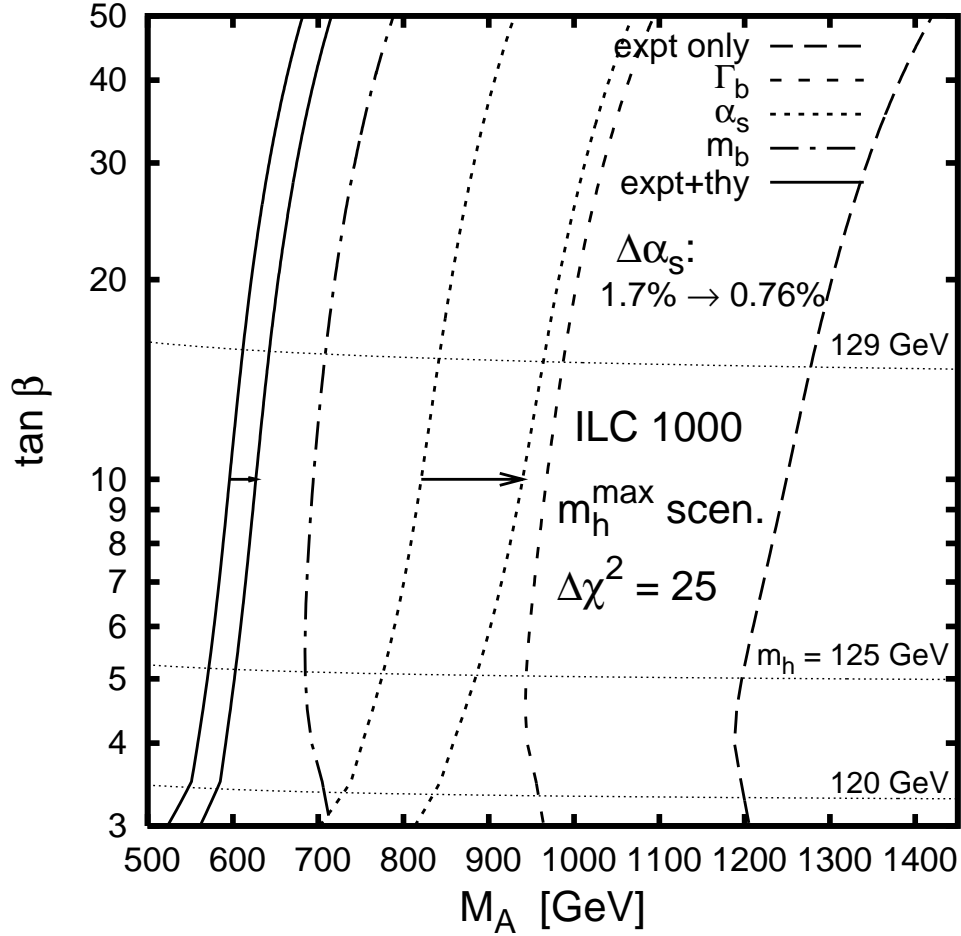


FIG. 6: Effect on the Phase 2 $\Delta\chi^2 = 25$ contours of improving the uncertainty on $\alpha_s(m_Z)$ from 1.7% to 0.76%, as projected for GigaZ in Ref. [1].

Determining which part of these processes should be included in the $H \rightarrow gg$ branching fraction and which in the $H \rightarrow c\bar{c}$ or $b\bar{b}$ branching fractions will require interaction between the theoretical and experimental studies. The impact of this splitting on the $b\bar{b}$ final state is small, but it could potentially shift the numbers of events tagged as $c\bar{c}$ or gg by tens of percent (see the end of Appendix A 4 for details). We have not attempted to address this question here.

To understand the effect of the correlated uncertainties, we recall that for large $\tan\beta$, Γ_b and Γ_τ exhibit the largest deviations from their SM values, while Γ_W approaches its SM value very quickly with increasing M_A [Eq. (3)]. The largest parametric and theoretical uncertainties appear in the hadronic decay widths of the Higgs. At the same time, the most precisely measured observables in Phase 2 of the ILC are $\sigma \times \text{BR}(bb)$ and $\sigma \times \text{BR}(gg)$, which suffer directly from the parametric and theoretical uncertainties, and $\sigma \times \text{BR}(WW)$, which

is affected indirectly through the Higgs total width. Adding a high-precision measurement of $\sigma \times \text{BR}(\tau\tau)$ would allow a tight constraint on the MSSM Higgs unpolluted by the dominant uncertainties. This mode is affected by the parametric and theoretical uncertainties indirectly through the Higgs total width in the same way as $\sigma \times \text{BR}(WW)$, so that the ratio of these two non-hadronic modes is relatively clean. Further, Γ_τ exhibits a large deviation from its SM value in the MSSM [see Eq. (3)], leading to good potential sensitivity to the MSSM nature of the Higgs.

To illustrate the potential improvement, we first note that for m_H between 120 and 140 GeV, the experimental uncertainties in the $b\bar{b}$, WW , and gg final states improve by factors of 5–6, 4–5, and 3.5–5.5, respectively, between Phase 1 and Phase 2 (see Tables I and II). We thus expect that an improvement in the $\tau\tau$ final state in Phase 2 by a factor of about four should be reasonable, and show the impact of a measurement of $\sigma \times \text{BR}(\tau\tau)$ with an uncertainty of 1.3% (2.0%) at $m_H = 120$ (140) GeV in Fig. 7. The effect of such a measurement on the reach in M_A including only experimental uncertainties is minor, because the precision assumed here is not particularly high compared to that of $\sigma \times \text{BR}(b\bar{b})$ and $\sigma \times \text{BR}(WW)$. However, the impact on the reach including parametric and theoretical uncertainties is quite significant, improving the reach from ~ 600 GeV to ~ 800 GeV. A measurement of $\sigma \times \text{BR}(\tau\tau)$ would require a different selection than used in Ref. [15], which required the visible energy in the event to add up to the Higgs mass; in the case of $H \rightarrow \tau\tau$, some energy is lost through the neutrinos in the τ decays.

As the experimental studies for the ILC Higgs measurements are refined, we hope that the correlations among the experimental uncertainties in different channels will be quantified. In particular, we expect the hadronic decay modes $H \rightarrow gg$, $b\bar{b}$ and $c\bar{c}$ to be correlated, because the separation of these three channels relies on bottom and charm tagging. Because the shifts in Higgs observables in particular models are correlated due to the model structure, we expect the correlations in the experimental uncertainties to be important for evaluating model distinguishability. Once these correlated uncertainties are available, including them in a χ^2 framework will be straightforward.

We used the m_h^{max} benchmark scenario of the MSSM to quantify the impact of the theoretical and parametric uncertainties. Our analysis can be extended in a straightforward way to Higgs coupling comparisons in other scenarios of the MSSM and to other beyond-the-SM Higgs sectors. Such a study would be interesting because the characteristic deviations from

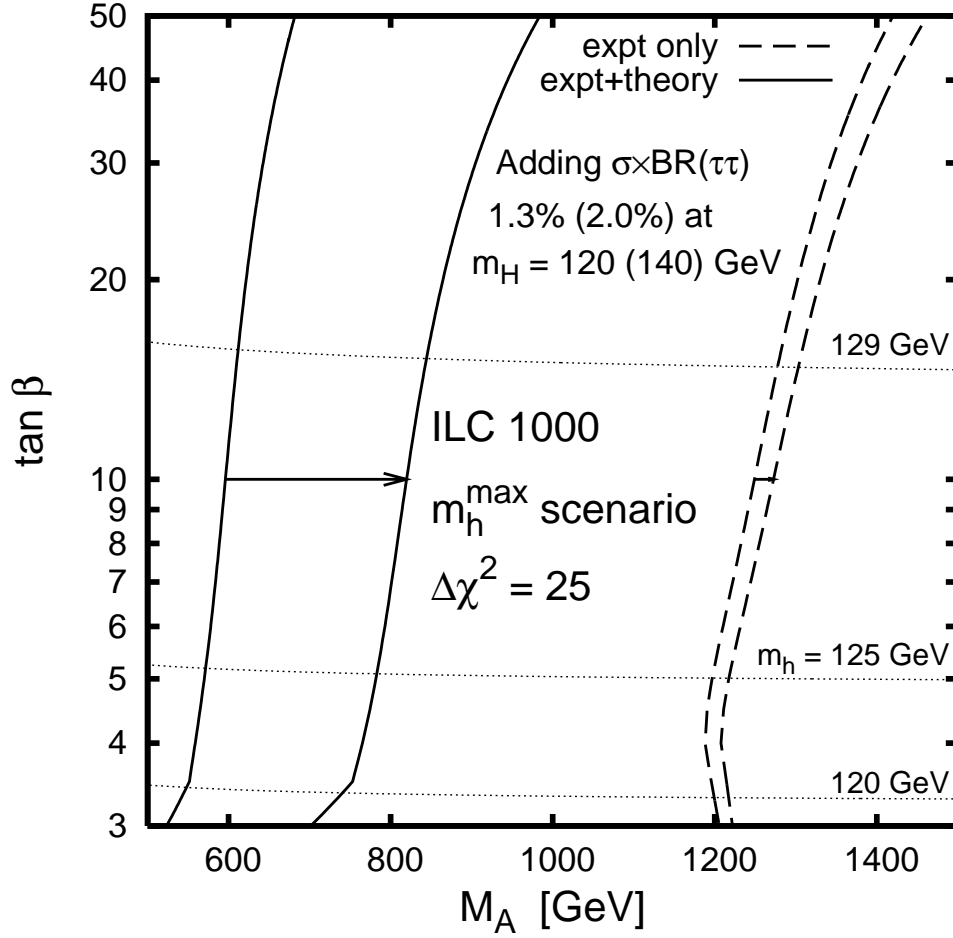


FIG. 7: Effect on the Phase 2 $\Delta\chi^2 = 25$ contours of adding a measurement of $\sigma \times \text{BR}(\tau\tau)$ with a precision of 1.3% (2.0%) at $m_H = 120$ (140) GeV.

the SM in different extended models may appear in different channels than for the MSSM m_h^{max} scenario, so that the relative importance of the various Higgs measurements will differ. Further, the shifts in the observables predicted in different extended Higgs models may pull in different directions relative to the correlations in the uncertainties in the SM predictions.

Acknowledgments

We are grateful to Tim Barklow and Klaus Desch for clarifying the experimental studies of Higgs production and decay at the ILC, to Stefan Dittmaier for an enlightening discussion on the high-precision calculation of the $e^+e^- \rightarrow \nu\bar{\nu}H$ cross section, and to Thomas Becher, Andre Hoang, Andreas Kronfeld and Frank Petriello for useful conversations on the bottom and charm quark mass uncertainties. This work was supported by the Natural Sciences and

Engineering Research Council of Canada.

APPENDIX A: THEORETICAL UNCERTAINTIES IN HIGGS DECAY PARTIAL WIDTHS

The radiative corrections to Higgs decays have been reviewed in Ref. [16]; we give here a brief sketch of the known corrections. The theory uncertainties used in our analysis were summarized in Table III.

1. $H \rightarrow q\bar{q}$

The QCD corrections to $H \rightarrow q\bar{q}$ are known up to three loops (N³LO) [23, 24, 25] for massless final-state quarks. A compact formula in the $\overline{\text{MS}}$ scheme is given in Ref. [16]:

$$\Gamma(H \rightarrow q\bar{q}) = \frac{3G_F m_H}{4\sqrt{2}\pi} \overline{m}_q^2(m_H) [\Delta_{\text{QCD}} + \Delta_t], \quad (\text{A1})$$

where

$$\begin{aligned} \Delta_{\text{QCD}} &= 1 + 5.67 \frac{\alpha_s(m_H)}{\pi} + (35.94 - 1.36N_F) \left(\frac{\alpha_s(m_H)}{\pi} \right)^2 \\ &\quad + (164.14 - 25.77N_F + 0.259N_F^2) \left(\frac{\alpha_s(m_H)}{\pi} \right)^3 \\ &\simeq 1 + 0.20 + 0.04 + 0.003 \\ \Delta_t &= \left(\frac{\alpha_s(m_H)}{\pi} \right)^2 \left[1.57 - \frac{2}{3} \log \frac{m_H^2}{M_t^2} + \frac{1}{9} \log^2 \frac{\overline{m}_q^2(m_H)}{m_H^2} \right] \\ &\simeq 0.02. \end{aligned} \quad (\text{A2})$$

In this calculation, the $\overline{\text{MS}}$ running quark masses $\overline{m}_q(M_q)$ evaluated at the quark pole mass M_q are taken as a starting point and then run up to the Higgs mass scale using the standard QCD running in order to absorb large logarithms. The coefficient functions for the running of the quark masses are known to four-loop accuracy [26], as is the beta-function for the running of α_s [27]. We thus estimate the uncertainty in the partial width from the running of $\overline{m}_q(m_H)$ to be well below the 0.01% level.

The perturbative expansion for Δ_{QCD} in Eq. (A2) is well under control; Δ_t appears at NNLO and is roughly the same size as the NNLO term in Δ_{QCD} . We thus estimate the

uncertainty from uncalculated higher-order QCD corrections to be smaller than the last calculated term in each series: $\sim 0.1\%$ from Δ_{QCD} and $\sim 1\%$ from Δ_t .

We note here that an additional contribution to $H \rightarrow q\bar{q}$ can come from $H \rightarrow gg^*$ with the off-shell gluon splitting to $q\bar{q}$; we have *not* included these effects in our calculations. See Sec. A 4 for further discussion.

For Higgs decays to heavy quarks near the threshold region, the quark pole mass dependence must be included through the usual $\beta^3 = (1 - 4M_q^2/m_H^2)^{3/2}$ factor. The NLO QCD corrections for massive quarks are known [23], as is the $\mathcal{O}(N_f\alpha_s^2)$ piece of the massive NNLO corrections [28]. HDECAY uses a linear interpolation between the NLO massive and the N³LO massless results near the threshold region [16]. For $m_H \sim 120$ GeV, the quark mass effects decrease the $H \rightarrow b\bar{b}$ ($c\bar{c}$) partial width by about 0.7% (0.1%). We estimate the remaining uncertainty from quark mass effects in the QCD corrections to be below the 0.01% level.

The electroweak corrections to the Higgs decay into fermion pairs are known at one loop [29, 30]; a convenient approximation formula is given in Refs. [16, 31]. The QED corrections include a large logarithm $\log(m_H^2/M_q^2)$, which can be absorbed into the running fermion mass as in QCD. The electroweak corrections also include a top-mass-dependent piece which increases the $H \rightarrow q\bar{q}$ partial width by about 2.2% for decays to $c\bar{c}$ and by 0.3% for decays to $b\bar{b}$ (the difference is due to the vertex correction involving a top quark in the case of $b\bar{b}$, which partly cancels the universal correction). In addition, the two- and three-loop QCD corrections to the top-mass-dependent piece of the electroweak correction are known [32, 33]. Their numerical size depends on the scheme chosen to define the running α_s and top quark mass [33]; a suitable choice gives a *relative* correction to the top-mass-dependent piece of the NLO electroweak correction of 8% (two-loop) and 1% (three-loop). The remaining electroweak corrections are comparable in size, i.e., at the percent level. We thus estimate the remaining theoretical uncertainty from higher-order electroweak and mixed electroweak/QCD corrections to be smaller by a loop factor $\sim \alpha/\pi$, i.e., at the level of 0.01%.

For large Higgs masses, electroweak corrections due to the Higgs self-coupling become relevant. These were calculated in Ref. [34] and can increase $\Gamma_{q\bar{q}}$ by about 2% for $m_H \sim 1$ TeV. For a 120 GeV Higgs, they increase $\Gamma_{q\bar{q}}$ by about 0.2% at NLO and by another -0.002% at NNLO. Any remaining uncertainty from higher orders in the Higgs self-coupling is thus totally negligible in the intermediate Higgs mass range.

We thus estimate the theory uncertainty in $\Gamma_{b\bar{b}}$ and $\Gamma_{c\bar{c}}$ to be at the 1% level, primarily from the Δ_t piece of the QCD corrections.

2. $H \rightarrow \ell^+ \ell^-$

Higgs decays to leptons receive the same electroweak corrections as the decays to quarks discussed in the previous section. As mentioned previously, we estimate that the theoretical uncertainty is at the level of two-loop electroweak corrections $\sim (\alpha/\pi)^2 \sim 0.01\%$.

3. $H \rightarrow WW, ZZ$

For Higgs masses below the WW threshold, decays with one or both gauge bosons off-shell are important, with branching ratios for the doubly off-shell decays reaching the percent level for Higgs masses above about 100–110 GeV [16]. Until recently, calculations for off-shell vector bosons were only available at tree level, and radiative corrections to Higgs decays to WW and ZZ were known only in the narrow-width approximation. In this approximation, the one-loop electroweak corrections [29, 35, 36, 37] amount to about 5% or less in the intermediate mass range [16]. Furthermore, the QCD corrections to the leading top-mass-enhanced electroweak corrections of $\mathcal{O}(\alpha_s G_F m_t^2)$ have been calculated at two [38, 39] and three [40, 41] loops; these mixed electroweak/QCD corrections amount to roughly 0.5%. **HDECAY** takes into account both singly off-shell and doubly off-shell decays at tree level but neglects these electroweak and mixed corrections [16].

Recently the complete NLO strong and electroweak radiative corrections for $H \rightarrow WW/ZZ \rightarrow 4f$ have been calculated including the effects of off-shell gauge bosons [42, 43]. The calculation was improved by including final-state photon radiation off the fermions, resummed using a structure function approach, as well as higher-order corrections due to the Higgs self-coupling relevant for large Higgs masses [45, 46], which increase the decay width for a 120 GeV Higgs by about 0.2% at NLO and by another 0.003% at NNLO. The complete calculation has been implemented in the Monte Carlo generator **PROPHECY4F** [42, 43]. For Higgs masses below 400 GeV, the theoretical uncertainty is below 1%; for our study we estimate the theory uncertainty in Γ_{WW} and Γ_{ZZ} in the intermediate Higgs mass range to be at the 0.5% level [44].

4. $H \rightarrow gg$

The decay $H \rightarrow gg$ appears first at one-loop mediated by a quark triangle. The top quark loop dominates the amplitude because it contributes proportional to the large top Yukawa coupling $y_t = gm_t/\sqrt{2}m_W \sim 1$. The bottom quark loop is also included in **HDECAY**; it reduces the $H \rightarrow gg$ partial width by about 11% for $m_H = 120$ GeV compared to including the top loop alone. We note that **HDECAY** v.3.103 [13] (downloaded June 2006) includes the charm quark loop in the calculation of the MSSM $h^0 \rightarrow gg$ partial width, but not in the calculation of the SM $H \rightarrow gg$ partial width. For consistency, we add the charm loop into the SM $H \rightarrow gg$ calculation; it reduces Γ_{gg} by about 2% for $m_H = 120$ GeV.³

The QCD corrections to $H \rightarrow gg$ are most easily calculated in the heavy quark limit, in which $m_t \rightarrow \infty$ is taken in the leading-order top triangle diagram (the amplitude goes to a constant in this limit). This allows the top triangle to be shrunk to a point and replaced with an effective coupling of the Higgs to two gluons. **HDECAY** includes the NLO QCD correction to Γ_{gg} in this heavy quark limit only; in the intermediate Higgs mass range this correction shifts Γ_{gg} upward by about 60–65% relative to the leading-order (LO) partial width. The NLO QCD corrections with full dependence on the mass of the quark in the loop are known [47]; in the intermediate Higgs mass range, including the full mass dependence shifts Γ_{gg} upward by an additional 5% of the LO width [16]. This mass-dependent part of the correction is not included in **HDECAY**.

The NNLO QCD correction is known only in the heavy quark limit [48]; it adds an additional 20% to the LO result. Very recently, the N³LO QCD corrections to Γ_{gg} have been computed [49], again in the heavy quark limit; they add another 2% to the LO result. By varying the renormalization scale between $m_H/2$ and $2m_H$, a measure of the theoretical uncertainty of the calculation can be estimated: the scale dependence decreases from 24% (LO) to 22% (NLO) to 10% (NNLO), and finally to only 3% at N³LO [49]. Neglecting the mass dependence of the NLO correction and neglecting the NNLO and N³LO corrections entirely leaves **HDECAY** with about a 16% relative uncertainty on the calculated NLO partial width.

The electroweak corrections of $\mathcal{O}(G_F m_t^2)$ to $H \rightarrow gg$ were calculated in [50] in the heavy-

³ This number is for **NF-GG** = 5, i.e., the gluon splitting to $b\bar{b}$ or $c\bar{c}$ at NLO is *not* subtracted off Γ_{gg} and added on to $\Gamma_{b\bar{b}, c\bar{c}}$; see the end of this subsection for further discussion of this issue.

top approximation and they give a simple multiplicative factor which increases the gluonic decay width by about 0.3%. We thus expect the NNLO electroweak corrections and the NLO finite-top-mass effects to be below the per-mille level. This NLO electroweak correction is neglected in **HDECAY**.

We thus take the remaining theory uncertainty in Γ_{gg} to be roughly 3%, corresponding to the scale uncertainty in the N³LO QCD calculation.

Finally, we note here a potential issue for the theoretical interpretation of Higgs partial width measurements that requires further study. Theoretical calculations of the higher-order QCD corrections to $H \rightarrow gg$ include processes in which one of the final-state gluons splits into a quark-antiquark pair. The **HDECAY** code contains a switch that allows the user to specify the number of final-state quark flavours included in Γ_{gg} ; setting **NF-GG** = 5 includes the five light quark flavours in Γ_{gg} , while **NF-GG** = 4 separates off the contribution from gluon splitting to $b\bar{b}$ and adds it in to $\Gamma_{b\bar{b}}$. **NF-GG** = 3 does the same for gluon splitting to $c\bar{c}$ as well.

Compared to **NF-GG** = 5 and for $m_H = 120$ GeV, subtracting off the gluon splitting to $b\bar{b}$ and adding it to $\Gamma_{b\bar{b}}$ (i.e., **NF-GG** = 4) raises $\Gamma_{b\bar{b}}$ by about 1% and reduces Γ_{gg} by about 9%. Subtracting off the gluon splitting to $c\bar{c}$ and adding it to $\Gamma_{c\bar{c}}$ (i.e., **NF-GG** = 3) raises $\Gamma_{c\bar{c}}$ by almost 30% and reduces Γ_{gg} by a further 12%. These effects are quite significant compared to the expected experimental precision in the gg and $c\bar{c}$ channels. The amount of this gluon splitting correction that should be subtracted off of Γ_{gg} and included in $\Gamma_{b\bar{b}}$ or $\Gamma_{c\bar{c}}$ is an experimental question requiring a more detailed simulation of flavour tagging of Higgs decays into three-body final states. In our study we set **NF-GG** = 5 throughout and ignore this issue.

5. $H \rightarrow \gamma\gamma$

The SM $H \rightarrow \gamma\gamma$ decay partial width receives QCD corrections to the one-loop diagrams involving quarks. Because the external particles in the $H\gamma\gamma$ vertex are colour neutral, the virtual QCD corrections are finite by themselves. The QCD corrections to the top quark loop in $\Gamma_{\gamma\gamma}$ are known analytically at NLO [51] and as a power expansion up to third order in m_H/m_t at NNLO [52]. The NLO corrections are of order 2% for $m_H < 2m_W$, and the NNLO corrections are at the level of a few per mille. These QCD corrections are neglected [16] in

HDECAY.

$\Gamma_{\gamma\gamma}$ also receives electroweak corrections, the complete set of which have been calculated at NLO neglecting the Yukawa couplings of all fermions except the top quark. The complete calculation consists of the two-loop diagrams containing light fermion loops and W or Z bosons (with the Higgs coupled to the W or Z , because the light fermion Yukawa couplings are neglected) [53]; the two-loop diagrams involving third-generation quarks and electroweak bosons [54, 55, 56]; and the purely bosonic corrections [56]. Together, these NLO electroweak corrections are between -4% and 0% for $100 \text{ GeV} \lesssim m_H \lesssim 150 \text{ GeV}$. These electroweak corrections are neglected [16] in HDECAY.

The corrections to the part of the $H \rightarrow \gamma\gamma$ amplitude involving the Higgs coupling to light quarks (e.g., b) have not been computed. However, since the leading order contribution of the b quark loop to $\Gamma_{\gamma\gamma}$ is at the few percent level, and the QCD and electroweak radiative corrections are themselves at the few percent level of the leading order piece, we estimate these uncalculated two-loop corrections to be at most at the per-mille level. We thus take the remaining theoretical uncertainty in $\Gamma_{\gamma\gamma}$ to be of order 0.1% .

6. $H \rightarrow Z\gamma$

Like $H \rightarrow \gamma\gamma$, the SM $H \rightarrow Z\gamma$ decay partial width receives QCD corrections to the one-loop diagrams involving quarks. These corrections were given in Ref. [57] including the full dependence on the Higgs, Z and top quark masses. They amount to less than 0.3% in the intermediate Higgs mass range [16] and have been neglected in HDECAY.

In analogy with the $H \rightarrow \gamma\gamma$ process, we expect the two-loop electroweak corrections to $\Gamma_{Z\gamma}$ to be at the few-percent level; we thus take an overall theory uncertainty of 4% for the $H \rightarrow Z\gamma$ mode.

APPENDIX B: THEORETICAL UNCERTAINTY IN THE $e^+e^- \rightarrow \nu\bar{\nu}H$ PRODUCTION CROSS SECTION

The full one-loop electroweak radiative corrections to Higgs production via $e^+e^- \rightarrow \nu\bar{\nu}H$ have been calculated in Refs. [17, 18, 19]. For the experimental selection used in the 1000 GeV centre-of-mass energy ILC studies [15], the processes $e^+e^- \rightarrow \nu_\ell\bar{\nu}_\ell H$ ($\ell = e, \mu, \tau$)

arising from both WW fusion and Higgsstrahlung contribute, with WW fusion dominating. The one-loop electroweak corrections to these processes reduce the cross section by about 10% [18, 19] in the parameter range of interest to us.

Beyond one loop, the $e^+e^- \rightarrow \nu\bar{\nu}H$ cross section will receive additional electroweak and QCD corrections. We estimate the missing two-loop electroweak corrections to be roughly of order (one-loop)². The largest electroweak corrections are due to initial-state radiation, which is already computed in the leading-log approximation up to order α^3 [19]. The remaining purely weak one-loop corrections are of order 3–4% [19], leading us to estimate a (one-loop)² uncertainty of about 0.1–0.2%. At two loops, QCD corrections will affect only the fermionic component of the one-loop electroweak corrections; this fermionic component amounts to about a 2% reduction of the total cross section in our parameter region of interest [18], so we estimate the QCD correction at two loops to be of order 0.2%. At TeV energies one should also consider the enhanced effects that often occur in high-energy ($E \gg m_W$) processes, such as logarithmic running of couplings and soft or collinear weak boson exchange; these effects can be at the percent level even at two loops. However, the t -channel weak boson fusion process of interest here is dominated by small energy transfers, so that we do not expect these effects to exceed the 0.1% level. For a relatively light Higgs mass $m_H \sim 120\text{--}140$ GeV the Higgs self-coupling is relatively small, so that we should also be safe from large corrections due to Higgs self-interaction diagrams at the two-loop level.

We thus estimate a combined theory uncertainty on the $e^+e^- \rightarrow \nu\bar{\nu}H$ cross section at 1000 GeV centre-of-mass energy of 0.5% [44]. We emphasize that this is just a “reasonable” estimate; to make this number really solid would require a serious study of the size of the two-loop effects mentioned above.

APPENDIX C: UNCERTAINTIES IN $\overline{m}_b(\overline{m}_b)$ AND $\overline{m}_c(\overline{m}_c)$

The predictions for the Higgs partial widths into bottom or charm quark pairs are computed up to three loops in terms of the $\overline{\text{MS}}$ quark masses evaluated at the scale of the Higgs mass. As input, the calculation requires the bottom and charm quark $\overline{\text{MS}}$ masses at a starting scale such as the quark’s own mass: $\overline{m}_b(\overline{m}_b)$ and $\overline{m}_c(\overline{m}_c)$. We summarize here the various ways that $\overline{m}_b(\overline{m}_b)$ and $\overline{m}_c(\overline{m}_c)$ have been extracted; the masses obtained are summarized in Tables VIII and IX.

Source	$\overline{m}_c(\overline{m}_c)$ [GeV]
Inclusive semileptonic B decays	
via m_b^{1S} and $m_b - m_c$ [22]	1.224 ± 0.057 (*)
via kinetic masses [21]	1.24 ± 0.07
$e^+e^- \rightarrow$ hadrons	
from spectral moments [62]	1.304 ± 0.027
more conservative error analysis [61]	1.29 ± 0.07
Quenched lattice QCD	
from F_K and D_s mass [65]	$1.301 \pm 0.034 \pm ??$
from $\bar{c}c$ and $\bar{c}s$ state masses [66]	$1.319 \pm 0.028 \pm ??$
Unquenched lattice QCD	
meson spectra (prelim) [68]	1.22 ± 0.09

TABLE VIII: $\overline{\text{MS}}$ charm quark masses, $\overline{m}_c(\overline{m}_c)$, from recent analyses (see text for details). In our study we use the charm mass extracted from inclusive semileptonic B decays [22], marked with an asterisk (*) in the table. For quenched lattice QCD the question marks ?? denote the uncontrolled uncertainty due to the quenched approximation.

Source	$\overline{m}_b(\overline{m}_b)$ [GeV]
Inclusive semileptonic B decays	
via kinetic masses [21]	4.20 ± 0.04 (*)
$e^+e^- \rightarrow$ hadrons	
from spectral moments [62]	4.191 ± 0.051
more conservative error analysis [61]	4.22 ± 0.11
Quenched lattice QCD	
from $\bar{b}b$ and $\bar{b}s$ state masses [66]	$4.33 \pm 0.10 \pm ??$
Unquenched lattice QCD	
Υ spectrum [67]	4.4 ± 0.3
meson spectra (prelim) [68]	4.7 ± 0.4

TABLE IX: $\overline{\text{MS}}$ bottom quark masses, $\overline{m}_b(\overline{m}_b)$, from recent analyses (see text for details). In our study we use the bottom mass extracted from inclusive semileptonic B decays [21], marked with an asterisk (*) in the table. For quenched lattice QCD the question marks ?? denote the uncontrolled uncertainty due to the quenched approximation.

Extracting the precise values of the charm and bottom quark masses from experiment is a challenge because of QCD effects which are starting to become strong at the bottom and charm mass scales. In particular, perturbative QCD does not allow one to define the quark pole masses with an accuracy better than $\Lambda_{\text{QCD}} \sim 200$ MeV; this is known as the

renormalon ambiguity.⁴ Because the $\overline{\text{MS}}$ quark masses are short-distance mass definitions, they are in principle free of this ambiguity.

1. Inclusive semileptonic B decays

The charm mass has recently been extracted [22] from a global fit to B meson decay spectra [58]. The procedure combines the values of $m_b - m_c$ and $m_b^{1\text{S}}$ from a fit of the decay spectra of $B \rightarrow X_c \ell \bar{\nu}$ and $B \rightarrow X_s \gamma$ to a Heavy Quark Effective Theory (HQET) expansion performed in Ref. [58]. The proper treatment of the renormalon cancellation was done in Ref. [22] to extract the charm mass $\overline{m}_c(\overline{m}_c) = 1.224 \pm 0.017_{\text{expt}} \pm 0.054_{\text{thy}}$ GeV, where the first error is experimental and includes the uncertainty in α_s and the second error represents a conservative combination of the theory uncertainties in the extraction [22]. While this theory uncertainty is not meant to be interpreted as a statistical uncertainty (it represents a range where the true charm mass should be located with probability much higher than the 67% probability of a 1σ interval), we will nevertheless treat it as a 1σ Gaussian error and combine it in quadrature with the experimental error for inclusion in our χ^2 fits. For our analysis we thus take a charm mass of

$$\overline{m}_c(\overline{m}_c) = 1.224 \pm 0.057 \text{ GeV.} \quad (\text{C1})$$

The quoted uncertainty amounts to a 4.7% relative uncertainty, which is dominated by the theoretical uncertainty. The theoretical uncertainty could be improved in the future by a full $\mathcal{O}(\alpha_s^2)$ analysis of the inclusive B decay spectra used in the extraction, to reduce the theoretical uncertainty in the fit to the HQET parameters.

The charm quark mass has also been extracted in Ref. [21] through a similar fit to the $B \rightarrow X_c \ell \bar{\nu}$ and $B \rightarrow X_s \gamma$ decay distributions using HQET expansions in the kinetic scheme, yielding kinetic masses m_b and m_c which are converted to $\overline{\text{MS}}$ masses using a formula from Ref. [59], accurate to two loops and including part of the three-loop α_s^3 corrections. The resulting $\overline{\text{MS}}$ charm mass is $\overline{m}_c(\overline{m}_c) = 1.24 \pm 0.07$ GeV. This is consistent within the

⁴ A renormalon is a power-like infrared-sensitive contribution to a hard process – a relative correction of order Λ_{QCD}/m_Q in our case – as opposed to the usual logarithmic infrared-sensitive effects $\log(\Lambda_{\text{QCD}}/m_Q)$ encountered in QCD calculations.

uncertainties with the charm mass found in Ref. [22].

The fits of the $B \rightarrow X_c \ell \bar{\nu}$ and $B \rightarrow X_s \gamma$ decay distributions to HQET expansions are also used to extract the bottom quark mass. The extraction can be done using any of a variety of different schemes for the HQET expansions [58]; however, some schemes are better than others in the sense that they suffer from smaller theoretical uncertainties. Currently the smallest uncertainty comes with the bottom mass extraction in the $1S$ scheme, $m_b^{1S} = 4.68 \pm 0.03$ GeV [58], an uncertainty of only 0.64%. The bottom mass has also been extracted [21, 58] in the kinetic scheme discussed above for the charm mass extraction. As for the charm quark, the kinetic bottom quark mass can be translated into an $\overline{\text{MS}}$ mass using the formula from Ref. [59]. Following this procedure, Ref. [21] finds for the $\overline{\text{MS}}$ mass,

$$\overline{m}_b(\overline{m}_b) = 4.20 \pm 0.04 \text{ GeV}. \quad (\text{C2})$$

We use this mass in our analysis. The relative uncertainty is 0.95%, and is dominated by the theoretical uncertainties that feed into the fit errors.

2. $e^+e^- \rightarrow \text{hadrons}$

The inclusive cross section for $e^+e^- \rightarrow \text{hadrons}$ as a function of the centre-of-mass energy is sensitive to the fundamental parameters of QCD, including the quark masses. In particular, precise perturbative QCD calculations of the first few “moments” of the cross section, which depend heavily on the threshold region, allow a precise determination of the $\overline{\text{MS}}$ charm and bottom quark masses.

The moments $P_n = \int R_{q\bar{q}}(s) s^{-(n+1)} ds$, where $R_{q\bar{q}} = \sigma(e^+e^- \rightarrow q\bar{q} + X)/\sigma(e^+e^- \rightarrow \mu^+\mu^-)$ and $q = c$ or b , are obtained experimentally from measurements of the production cross section near the $c\bar{c}$ and $b\bar{b}$ thresholds. Experimental uncertainties include gaps in the data above the quarkonium resonance regions and uncertainties in the large contributions from the narrow quarkonium resonances [60]. The quark masses are extracted by matching the experimentally determined moments to theoretical predictions. The uncertainties on the theory side include the unknown higher-order QCD contributions to the moments, which manifest both as scale dependence within a single scheme and differing results for the quark masses depending on how the renormalization scale is chosen as a function of the e^+e^-

centre-of-mass energy [61].

A recent fit [62] found $\overline{m}_c(\overline{m}_c) = 1.304 \pm 0.027$ GeV and $\overline{m}_b(\overline{m}_b) = 4.191 \pm 0.051$ GeV. This remarkably small error estimate for m_c was reconsidered in Refs. [60, 61], with special attention being paid to sources of theory uncertainty, resulting in revised mass extractions of $\overline{m}_c(\overline{m}_c) = 1.29 \pm 0.07$ GeV and $\overline{m}_b(\overline{m}_b) = 4.22 \pm 0.11$ GeV [61].

Very recently the first moment of the hadronic production cross section was computed at $\mathcal{O}(\alpha_s^3)$ [63, 64], significantly reducing the renormalization scale dependence. Repeating the analysis of Ref. [62], Ref. [64] finds $\overline{m}_c(\overline{m}_c) = 1.295 \pm 0.015$ GeV and $\overline{m}_b(\overline{m}_b) = 4.205 \pm 0.058$ GeV. We await a more detailed examination of the theoretical uncertainties a la Refs. [60, 61] before making use of this very small uncertainty in m_c .

3. Lattice QCD

Lattice QCD allows the extraction of the quark masses through fits of the fundamental QCD parameters – α_s and the quark masses – to precisely-measured meson properties such as the kaon mass and decay constant F_K (to set the QCD scale and the light quark masses) and the mass of the D_s meson (to provide sensitivity to the charm quark mass) [65]. Adding B mesons to the simulation allows access to the bottom quark mass [66]. The charm and bottom masses have been thus calculated in *quenched* lattice QCD, in which only virtual gluons are simulated and not virtual light-quark–antiquark pairs. Recent analyses find $\overline{m}_c(\overline{m}_c) = 1.301 \pm 0.034$ GeV [65] or 1.319 ± 0.028 GeV [66] and $\overline{m}_b(\overline{m}_b) = 4.33 \pm 0.10$ GeV [66]. However, quenched lattice QCD calculations suffer from an uncontrolled theoretical uncertainty due to the quenched approximation.

Unquenched lattice QCD simulations are significantly more computer-intensive and have only recently yielded significant results. The bottom quark mass in full (unquenched) lattice QCD was obtained for the first time in Ref. [67] from the Υ spectrum. The bare mass on the lattice was extracted with 1–2% uncertainty, which is mostly systematic and due to missing radiative corrections to the leading relativistic and discretization corrections to the Υ binding energies. The bare mass on the lattice depends on the lattice spacing, which cuts off the effective theory on the lattice; it can be converted to the $\overline{\text{MS}}$ mass without encountering infrared problems. The conversion is done at one loop yielding $\overline{m}_b(\overline{m}_b) = 4.4 \pm 0.3$ GeV [67], where the error is dominated by the perturbative uncertainty in the conversion from the bare

lattice mass. A two-loop calculation of the heavy quark self-energy to reduce the conversion error is underway [67]. Reducing the error in $\overline{m}_b(\overline{m}_b)$ to the level of the uncertainty in the bare lattice mass would make the lattice determination of $\overline{m}_b(\overline{m}_b)$ competitive with that from inclusive B meson decay distributions discussed above. A similar (preliminary) analysis [68] including also the charm quark gives $\overline{m}_c(\overline{m}_c) = 1.22 \pm 0.09$ GeV and $\overline{m}_b(\overline{m}_b) = 4.7 \pm 0.4$ GeV. These masses are all in good agreement within their uncertainties with the charm and bottom masses found through other techniques.

-
- [1] J. A. Aguilar-Saavedra *et al.* [ECFA/DESY LC Physics Working Group], arXiv:hep-ph/0106315.
 - [2] T. Abe *et al.* [American Linear Collider Working Group], in *Proc. of the APS/DPF/DPB Summer Study on the Future of Particle Physics (Snowmass 2001)* ed. N. Graf, arXiv:hep-ex/0106056.
 - [3] S. Heinemeyer *et al.*, arXiv:hep-ph/0511332.
 - [4] M. Battaglia, arXiv:hep-ph/9910271; M. Battaglia and K. Desch, arXiv:hep-ph/0101165.
 - [5] M. Carena, H. E. Haber, H. E. Logan and S. Mrenna, Phys. Rev. D **65**, 055005 (2002) [Erratum-ibid. D **65**, 099902 (2002)] [arXiv:hep-ph/0106116].
 - [6] J. Kamoshita, Y. Okada and M. Tanaka, Phys. Lett. B **391**, 124 (1997) [arXiv:hep-ph/9512307]; S. Kiyoura and Y. Okada, arXiv:hep-ph/0101172.
 - [7] J. Guasch, W. Hollik and S. Penaranda, Phys. Lett. B **515**, 367 (2001) [arXiv:hep-ph/0106027].
 - [8] S. Dawson and S. Heinemeyer, Phys. Rev. D **66**, 055002 (2002) [arXiv:hep-ph/0203067].
 - [9] H. E. Logan, Phys. Rev. D **70**, 115003 (2004) [arXiv:hep-ph/0405072].
 - [10] M. Carena, S. Heinemeyer, C. E. M. Wagner and G. Weiglein, Eur. Phys. J. C **26**, 601 (2003) [arXiv:hep-ph/0202167].
 - [11] H. E. Haber, arXiv:hep-ph/9501320.
 - [12] For a review and references, see M. Carena and H. E. Haber, Prog. Part. Nucl. Phys. **50**, 63 (2003) [arXiv:hep-ph/0208209].
 - [13] HDECAY version 3.103 (August 2005): A. Djouadi, J. Kalinowski and M. Spira, Comput. Phys. Commun. **108**, 56 (1998) [arXiv:hep-ph/9704448]. Code available from <http://people.web.psi.ch/spira/hdecay/>.

- [14] K. Desch [Higgs Working Group of the Extended ECFA/DESY Study], arXiv:hep-ph/0311092.
- [15] T. L. Barklow, arXiv:hep-ph/0312268.
- [16] M. Spira, Fortsch. Phys. **46**, 203 (1998) [arXiv:hep-ph/9705337].
- [17] G. Belanger, F. Boudjema, J. Fujimoto, T. Ishikawa, T. Kaneko, K. Kato and Y. Shimizu, Phys. Lett. B **559**, 252 (2003) [arXiv:hep-ph/0212261].
- [18] A. Denner, S. Dittmaier, M. Roth and M. M. Weber, Phys. Lett. B **560**, 196 (2003) [arXiv:hep-ph/0301189].
- [19] A. Denner, S. Dittmaier, M. Roth and M. M. Weber, Nucl. Phys. B **660**, 289 (2003) [arXiv:hep-ph/0302198].
- [20] S. Eidelman *et al.* [Particle Data Group], Phys. Lett. B **592**, 1 (2004).
- [21] O. Buchmüller and H. Flächer, Phys. Rev. D **73**, 073008 (2006) [arXiv:hep-ph/0507253].
- [22] A. H. Hoang and A. V. Manohar, Phys. Lett. B **633**, 526 (2006) [arXiv:hep-ph/0509195].
- [23] E. Braaten and J. P. Leveille, Phys. Rev. D **22**, 715 (1980); N. Sakai, Phys. Rev. D **22**, 2220 (1980); T. Inami and T. Kubota, Nucl. Phys. B **179**, 171 (1981); S. G. Gorishnii, A. L. Kataev and S. A. Larin, Sov. J. Nucl. Phys. **40**, 329 (1984) [Yad. Fiz. **40**, 517 (1984)]; M. Drees and K. i. Hikasa, Phys. Rev. D **41**, 1547 (1990); M. Drees and K. i. Hikasa, Phys. Lett. B **240**, 455 (1990) [Erratum-ibid. B **262**, 497 (1991)].
- [24] S. G. Gorishnii, A. L. Kataev, S. A. Larin and L. R. Surguladze, Mod. Phys. Lett. A **5**, 2703 (1990); Phys. Rev. D **43**, 1633 (1991); A. L. Kataev and V. T. Kim, Mod. Phys. Lett. A **9**, 1309 (1994); L. R. Surguladze, Phys. Lett. B **341**, 60 (1994) [arXiv:hep-ph/9405325]; K. G. Chetyrkin, J. H. Kuhn and A. K. Kwiatkowski, arXiv:hep-ph/9407271; K. G. Chetyrkin, Phys. Lett. B **390**, 309 (1997) [arXiv:hep-ph/9608318].
- [25] K. G. Chetyrkin and A. Kwiatkowski, Nucl. Phys. B **461**, 3 (1996) [arXiv:hep-ph/9505358]; S. A. Larin, T. van Ritbergen and J. A. M. Vermaseren, Phys. Lett. B **362**, 134 (1995) [arXiv:hep-ph/9506465].
- [26] K. G. Chetyrkin, Phys. Lett. B **404**, 161 (1997) [arXiv:hep-ph/9703278].
- [27] T. van Ritbergen, J. A. M. Vermaseren and S. A. Larin, Phys. Lett. B **400**, 379 (1997) [arXiv:hep-ph/9701390].
- [28] K. Melnikov, Phys. Rev. D **53**, 5020 (1996) [arXiv:hep-ph/9511310].
- [29] J. Fleischer and F. Jegerlehner, Phys. Rev. D **23**, 2001 (1981).
- [30] D. Y. Bardin, B. M. Vilensky and P. K. Khristova, Sov. J. Nucl. Phys. **53**, 152 (1991) [Yad.

- Fiz. **53**, 240 (1991)]; A. Dabelstein and W. Hollik, Z. Phys. C **53**, 507 (1992); B. A. Kniehl, Nucl. Phys. B **376**, 3 (1992).
- [31] A. Djouadi, D. Haidt, B. A. Kniehl, P. M. Zerwas and B. Mele, in the Proceedings of the Workshop on e^+e^- Collisions at 500 GeV: The Physics Potential, Munich/Annecy/Hamburg 1991, ed. P.M. Zerwas, Report DESY 92-123A.
 - [32] B. A. Kniehl and M. Spira, Nucl. Phys. B **432**, 39 (1994) [arXiv:hep-ph/9410319]; A. Kwiatkowski and M. Steinhauser, Phys. Lett. B **338**, 66 (1994) [Erratum-ibid. B **342**, 455 (1995)] [arXiv:hep-ph/9405308].
 - [33] K. G. Chetyrkin, B. A. Kniehl and M. Steinhauser, Phys. Rev. Lett. **78**, 594 (1997) [arXiv:hep-ph/9610456].
 - [34] A. Ghinculov, Phys. Lett. B **337**, 137 (1994) [Erratum-ibid. B **346**, 426 (1995)] [arXiv:hep-ph/9405394]; L. Durand, K. Riesselmann and B. A. Kniehl, Phys. Rev. Lett. **72**, 2534 (1994) [Erratum-ibid. **74**, 1699 (1995)]; L. Durand, B. A. Kniehl and K. Riesselmann, Phys. Rev. D **51**, 5007 (1995) [arXiv:hep-ph/9412311]; V. Borodulin and G. Jikia, Phys. Lett. B **391**, 434 (1997) [arXiv:hep-ph/9609447].
 - [35] B. A. Kniehl, Nucl. Phys. B **352**, 1 (1991).
 - [36] B. A. Kniehl, Nucl. Phys. B **357**, 439 (1991).
 - [37] D. Y. Bardin, P. K. Khristova and B. M. Vilensky, Sov. J. Nucl. Phys. **54**, 833 (1991) [Yad. Fiz. **54**, 1366 (1991)].
 - [38] B. A. Kniehl and M. Spira, Z. Phys. C **69**, 77 (1995) [arXiv:hep-ph/9505225].
 - [39] B. A. Kniehl and M. Spira, Nucl. Phys. B **443**, 37 (1995) [arXiv:hep-ph/9501392].
 - [40] B. A. Kniehl and M. Steinhauser, Phys. Lett. B **365**, 297 (1996) [arXiv:hep-ph/9507382].
 - [41] B. A. Kniehl and M. Steinhauser, Nucl. Phys. B **454**, 485 (1995) [arXiv:hep-ph/9508241].
 - [42] A. Bredenstein, A. Denner, S. Dittmaier and M. M. Weber, Phys. Rev. D **74**, 013004 (2006) [arXiv:hep-ph/0604011].
 - [43] A. Bredenstein, A. Denner, S. Dittmaier and M. M. Weber, arXiv:hep-ph/0611234.
 - [44] S. Dittmaier, private communication.
 - [45] A. Ghinculov, Nucl. Phys. B **455**, 21 (1995) [arXiv:hep-ph/9507240].
 - [46] A. Frink, B. A. Kniehl, D. Kreimer and K. Riesselmann, Phys. Rev. D **54**, 4548 (1996) [arXiv:hep-ph/9606310].
 - [47] M. Spira, A. Djouadi, D. Graudenz and P. M. Zerwas, Nucl. Phys. B **453**, 17 (1995)

- [arXiv:hep-ph/9504378].
- [48] K. G. Chetyrkin, B. A. Kniehl and M. Steinhauser, Phys. Rev. Lett. **79**, 353 (1997) [arXiv:hep-ph/9705240].
- [49] P. A. Baikov and K. G. Chetyrkin, Phys. Rev. Lett. **97**, 061803 (2006) [arXiv:hep-ph/0604194].
- [50] A. Djouadi and P. Gambino, Phys. Rev. Lett. **73**, 2528 (1994) [arXiv:hep-ph/9406432]; K. G. Chetyrkin, B. A. Kniehl and M. Steinhauser, Phys. Rev. Lett. **78**, 594 (1997) [arXiv:hep-ph/9610456]; K. G. Chetyrkin, B. A. Kniehl and M. Steinhauser, Nucl. Phys. B **490**, 19 (1997) [arXiv:hep-ph/9701277].
- [51] H. q. Zheng and D. d. Wu, Phys. Rev. D **42**, 3760 (1990); A. Djouadi, M. Spira, J. J. van der Bij and P. M. Zerwas, Phys. Lett. B **257**, 187 (1991); S. Dawson and R. P. Kauffman, Phys. Rev. D **47**, 1264 (1993); A. Djouadi, M. Spira and P. M. Zerwas, Phys. Lett. B **311**, 255 (1993) [arXiv:hep-ph/9305335]; K. Melnikov and O. I. Yakovlev, Phys. Lett. B **312**, 179 (1993) [arXiv:hep-ph/9302281]; M. Inoue, R. Najima, T. Oka and J. Saito, Mod. Phys. Lett. A **9**, 1189 (1994); J. Fleischer, O. V. Tarasov and V. O. Tarasov, Phys. Lett. B **584**, 294 (2004) [arXiv:hep-ph/0401090].
- [52] M. Steinhauser, arXiv:hep-ph/9612395.
- [53] U. Aglietti, R. Bonciani, G. Degrossi and A. Vicini, Phys. Lett. B **595**, 432 (2004) [arXiv:hep-ph/0404071]; Phys. Lett. B **600**, 57 (2004) [arXiv:hep-ph/0407162].
- [54] F. Fugel, B. A. Kniehl and M. Steinhauser, Nucl. Phys. B **702**, 333 (2004) [arXiv:hep-ph/0405232].
- [55] Y. Liao and X. y. Li, Phys. Lett. B **396**, 225 (1997) [arXiv:hep-ph/9605310]; A. Djouadi, P. Gambino and B. A. Kniehl, Nucl. Phys. B **523**, 17 (1998) [arXiv:hep-ph/9712330].
- [56] G. Degrossi and F. Maltoni, Nucl. Phys. B **724**, 183 (2005) [arXiv:hep-ph/0504137].
- [57] M. Spira, A. Djouadi and P. M. Zerwas, Phys. Lett. B **276**, 350 (1992).
- [58] C. W. Bauer, Z. Ligeti, M. Luke, A. V. Manohar and M. Trott, Phys. Rev. D **70**, 094017 (2004) [arXiv:hep-ph/0408002].
- [59] D. Benson, I. I. Bigi, T. Mannel and N. Uraltsev, Nucl. Phys. B **665**, 367 (2003) [arXiv:hep-ph/0302262].
- [60] G. Corcella and A. H. Hoang, Phys. Lett. B **554**, 133 (2003) [arXiv:hep-ph/0212297].
- [61] A. H. Hoang and M. Jamin, Phys. Lett. B **594**, 127 (2004) [arXiv:hep-ph/0403083].
- [62] J. H. Kühn and M. Steinhauser, Nucl. Phys. B **619**, 588 (2001) [Erratum-ibid. B **640**, 415

- (2002)] [arXiv:hep-ph/0109084].
- [63] K. G. Chetyrkin, J. H. Kuhn and C. Sturm, Eur. Phys. J. C **48**, 107 (2006) [arXiv:hep-ph/0604234].
- [64] R. Boughezal, M. Czakon and T. Schutzmeier, Phys. Rev. D **74**, 074006 (2006) [arXiv:hep-ph/0605023].
- [65] J. Rolf and S. Sint [ALPHA Collaboration], JHEP **0212**, 007 (2002) [arXiv:hep-ph/0209255].
- [66] G. M. de Divitiis, M. Guagnelli, R. Petronzio, N. Tantalo and F. Palombi, Nucl. Phys. B **675**, 309 (2003) [arXiv:hep-lat/0305018].
- [67] A. Gray, I. Allison, C. T. H. Davies, E. Gulez, G. P. Lepage, J. Shigemitsu and M. Wingate, Phys. Rev. D **72**, 094507 (2005) [arXiv:hep-lat/0507013].
- [68] M. Nobes and H. Trottier, PoS **LAT2005**, 209 (2006) [arXiv:hep-lat/0509128].